AD-A143 563 DETERMINATION OF SEA SURFACE TEMPERATURE WITH N-ROSS (NAVY-REMOTE OCEAN SENSING SYSTEM)(U) NAVAL RESEARCH LAB WASHINGTON DC J P HOLLINGER ET AL. 16 JUL 84 1/1

UNCLASSIFIED NRL-MR-5375 F/G 8/10 NL

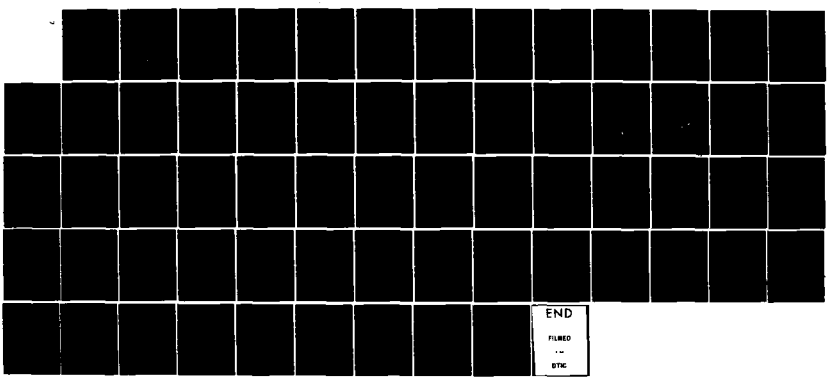

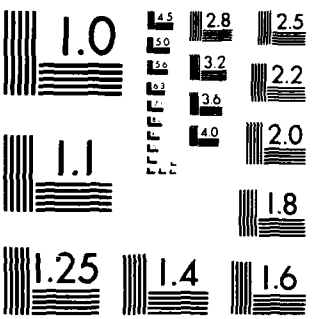

NRL Memorandum Report 5375

Determination of Sea Surface Temperature With N-ROSS

J. P. HOLLINGER AND R. C. LO

Space Sensing Applications Branch
Aerospace Systems Division

July 16, 1984

NAVAL RESEARCH LABORATORY
Washington, D.C.

SECURITY CLASSIFICATION OF THIS PAGE

REPORT DOCUMENTATION PAGE

1a REPORT SECURITY CLASSIFICATION UNCLASSIFIED	1b RESTRICTIVE MARKINGS
2a SECURITY CLASSIFICATION AUTHORITY	3 DISTRIBUTION/AVAILABILITY OF REPORT
2b DECLASSIFICATION/DOWNGRADING SCHEDULE	Approved for public release; distribution unlimited.
4 PERFORMING ORGANIZATION REPORT NUMBER(S) NRL Memorandum Report 5375	5. MONITORING ORGANIZATION REPORT NUMBER(S)
6a NAME OF PERFORMING ORGANIZATION Naval Research Laboratory 6b. OFFICE SYMBOL (If applicable) Code 7910	7a. NAME OF MONITORING ORGANIZATION
6c ADDRESS (City, State and ZIP Code) Washington, DC 20375	7b ADDRESS (City, State and ZIP Code)
8a. NAME OF FUNDING/SPONSORING ORGANIZATION Naval Air Systems Command 8b OFFICE SYMBOL (If applicable)	9. PROCUREMENT INSTRUMENT IDENTIFICATION NUMBER
8c ADDRESS (City, State and ZIP Code) Washington, DC 20361	10. SOURCE OF FUNDING NOS. PROGRAM ELEMENT NO: 63207N PROJECT NO: W0527 TASK NO: 3333OH/ 058C/ 4W05270S00 WORK UNIT NO: DN680-370
11 TITLE (Include Security Classification) Determination of Sea Surface Temperature with N-ROSS	
12 PERSONAL AUTHOR(S) Hollinger, J.P., and Lo, R.C.	
13a TYPE OF REPORT Final 13b. TIME COVERED FROM ~~10/83 to 9/84~~	14. DATE OF REPORT (Yr., Mo., Day) July 16, 1984 15 PAGE COUNT 64
16 SUPPLEMENTARY NOTATION	
17 COSATI CODES FIELD / GROUP / SUB GR	18. SUBJECT TERMS (Continue on reverse if necessary and identify by block number) Sea surface temperature Low frequency microwave radiometer (Continues)

19 ABSTRACT (Continue on reverse if necessary and identify by block number)

(+ or -)

The all-weather, global determination of sea surface temperature (SST) ~~has been~~ identified as a requirement needed to support Navy operations. The acceptable SST accuracy is ±1.0 K with a surface resolution of 25 km. Investigations of the phenomenology and technology of remote passive microwave sensing of the ocean environment over the past decade beginning with the Navy specification of the Remote Ocean-surface Measurement System ~~(ROMS)~~, through the NASA launched Scanning Multichannel Microwave Radiometer ~~(SMMR)~~ flown on both SEASAT and NIMBUS-7 to the planning by NASA of the Large Antenna Multichannel Microwave Radiometer ~~(LAMMR)~~, and development of the Mission Sensor Microwave/Imager (SSM/I) to be flown in 1985 by the Navy/Air Force, have demonstrated that this objective is presently attainable. Preliminary specifications and trade-off studies have been conducted to define the frequency, polarization, scan geometry, antenna size and other essential parameters, as well as the retrieval algorithms and spacecraft interface requirements, of the Low Frequency Microwave Radiometer (LFMR). As presently planned, the LFMR will be a stand alone system completely independent of the SSM/I but with a 30 rpm

(Continues)

20 DISTRIBUTION/AVAILABILITY OF ABSTRACT UNCLASSIFIED UNLIMITED X SAME AS RPT ☐ DTIC USERS ☐	21 ABSTRACT SECURITY CLASSIFICATION UNCLASSIFIED
22a NAME OF RESPONSIBLE INDIVIDUAL J. P. Hollinger	22b TELEPHONE NUMBER (Include Area Code) (202) 767-3398 22c OFFICE SYMBOL Code 7910

DD FORM 1473, 83 APR EDITION OF 1 JAN 73 IS OBSOLETE

SECURITY CLASSIFICATION OF THIS PAGE

18. SUBJECT TERMS (Continued)

N-ROSS
Antenna size
Baseline

19. ABSTRACT (Continued)

conical scan at 53.1° incidence angle identical to the SSM/I. It will be a dual-frequency system at 5.2 and 10.4 GHz using a 5.9 meter deployable mesh surface antenna. It is to be flown on the Navy-Remote Ocean Sensing System (N-ROSS) satellite scheduled to be launched in late 1988.

CONTENTS

DETERMINATION OF SEA SURFACE TEMPERATURE WITH N-ROSS

I. INTRODUCTION

The all-weather, global determination of sea surface temperature (SST) has been identified in the Satellite Measurement of Oceanographic Parameters Operational Requirement (SMOP OR-WO527-0S) as a requirement needed to support naval operations. The target SST accuracy is specified as $\pm$0.5 K at a surface resolution of 10 km with an accuracy of $\pm$1.0 K and surface resolution of 25 km acceptable. Passive microwave radiometry has the potential of meeting this requirement.

During the period 1972-78 NAVAIR supported inves'igations of the microwave radiometric properties of the ocean and atmosphere which led to the specification of the Remote Ocean-surface Measurement System (ROMS). Although ROMS was not built, the understanding of the phenomenology and technology developed for it directly contributed to subsequent systems.

NASA launched an experimental sensor, the Scanning Multichannel Microwave Radiometer (SMMR), on both the SEASAT and NIMBUS-7 satellites in 1978 to explore the all-weather measurement of sea surface temperature, as well as other oceanographic and atmospheric parameters, with microwave radiometry. The SMMR employs a 79 cm diameter antenna and dual-polarized radiometers at 6.6, 10.7, 18.0, 21.0, and 37 GHz with the 6.6 GHz frequency primarily chosen for its sensitivity to SST. Results from SMMR indicate that the SST can be measured to an RMS sensitivity $\pm$1.2 K or better with it, e.g. (1). However, the surface resolution of SMMR at 6.6 GHz is only 150 km.

The next generation of passive microwave sensors planned by NASA was the Large Antenna Multichannel Microwave Radiometer (LAMMR) as part of the sensor complement of the National Oceanic Satellite System (NOSS). LAMMR was planned as a seven-frequency, dual-polarized radiometric system with a four-meter antenna and a performance goal for SST of $\pm$0.5 K precision, $\pm$1.0 K absolute accuracy, and 24 to 36 km spatial resolution. Although NOSS and LAMMR were not built due to funding limitations, the design studies performed and the continuing development of the necessary technology have demonstrated that the SMOP OR is presently attainable.

The Navy-Remote Ocean Sensing System (N-ROSS) is a planned oceanographic satellite in the Navy core program for POM-84 with funding beginning in FY 85 to meet the SMOP OR. The sensor complement of N-ROSS is to include a scatterometer to measure the marine wind field; an altimeter to measure wave spectra, the earth's geoid, and to locate fronts and eddies; and a Mission Sensor Microwave/Imager (SSM/I) to measure sea ice, precipitation, atmospheric moisture, and surface winds. All-weather measurement of sea surface temperature will require the development of a

Manuscript approved April 24, 1984.

second passive microwave system. Critical to the development of this system is the selection of the operating frequency and other characteristics compatible with earth sources of RFI and optimized to functionally integrate with the SSM/I and N-ROSS.

The objective of this study is to define the frequency, antenna, and other essential parameters of a microwave radiometric system for the all-weather measurement of SST from N-ROSS.

II. SENSITIVITY AND RETRIEVAL ACCURACY STUDIES

A primary criterion for the selection of frequency for the low frequency microwave radiometer (LFMR) is sensitivity to, and thus the retrieval of, sea surface temperature (SST). The present sensitivity study will be limited to the frequency range of 2 to 14 GHz since frequencies below 2 GHz and above 14 GHz are relatively insensitive to SST (2). Three different approaches are used to examine the sensitivity question. They are (a) theoretical studies, (b) interpretation of satellite data, and (c) the use of aircraft data. The theoretical studies are the most versatile in that wide ranges of environmental conditions can be simulated, and many frequencies and frequency combinations can be examined. Functional relationships are built into the theoretical models providing the freedom to examine various trade-off relationships. Satellite and aircraft data, have, of course, the advantage of being actual measurements. They are, however, restricted in frequency and range of environmental conditions. The combination of all three studies provides a more complete basis for the determination of the microwave radiometric sensitivity to SST.

II.A. Theoretical Studies of Sensitivity

The rate of change of brightness temperature with respect to sea surface temperature, calculated using the geophysical model (3) developed at NRL, is given in Figure 1 as a function of frequency for several mean sea surface temperatures. The climatology (4) of the ocean-atmosphere system used with the model was compiled for mid-latitude summer conditions. The calculations are for vertical polarization of an incidence angle of 53.1°. All the parameters of the ocean-atmosphere system are kept constant except the SST for the calculation of the derivative.

The sensitivity is much greater over the frequency range of 6 to 10 GHz for very warm water, i.e., a SST of 30 C. However, the sensitivity decreases drastically, especially at the higher end of the frequency range, as the water temperature becomes colder. At 10 GHz and beyond, little sensitivity remains for the colder SST values. The sensitivity trend is reversed at the lower end of the frequency range, e.g. between 2 and 3 GHz. These frequencies are more sensitive to colder than to warmer water. Judging from Figure 1 the optimal frequency range for overall sensitivity appears to be in the 4 to 6 GHz range.

The choice of an optimum frequency not only depends on the sensitivity to SST but also on the sensitivity to other environmental parameters. If a given frequency is more sensitive to another parameter, such as wind speed, it will primarily provide information concerning that parameter rather than SST, even though the sensitivity to SST may also be significant. Some of

the most significant geophysical parameters for the microwave frequency range of interest are salinity, SST, wind speed, integrated atmospheric liquid water (clouds), and integrated atmospheric water vapor. The changes in the vertically polarized brightness temperature as a function of frequency is depicted in Figure 2 for those geophysical parameters. The incidence angle used in the calculations is again chosen to be the same as that of the SSM/I instrument, 53.1°, since there are advantages to choosing the same scan geometry for the LFMR because of possible mutual support and applications between the two instruments. The sensitivity to SST is dominant between about 2 and 10 GHz. Above about 10 GHz the effects due to water, both liquid and vapor, exceed that of SST while below about 2 GHz salinity effects are greater.

However, in order to examine the true relative sensitivity to various environmental parameters, the brightness temperature change caused by representative changes in the other relevant parameters must be examined. Assuming that the Navy's operational requirement for the other parameters are met, i.e., residual errors of $\frac{1}{2}$ part per thousand for salinity, 2 m/sec for surface wind speed, 0.01 gm/cm^2 for columnar density of liquid water, and 0.2 gm/cm^2 for columnar density of water vapor along with the minimum requirement of 1 C for SST, the corresponding resultant changes in brightness temperature were calculated. These changes in brightness temperature are given in Figure 3. As to be expected from Figure 2 the salinity effect ceases to be significant for frequencies higher than about 3 GHz, and the vertically polarized brightness temperature is relatively insensitive to wind speed and water vapor. Liquid water is the only serious contender with SST for sensitivity and then only at the higher frequencies, above about 10 GHz.

Similar calculations are presented for the horizontally polarized brightness temperature in Figure 4. Wind speed and liquid water are the dominating environmental parameters. The sensitivity to water vapor is also higher than that of SST beyond 11 GHz. Thus, horizontal polarization primarily contains information concerning wind speed and liquid water. It therefore provides a means to remove the effect of these parameters from the vertically polarized brightness temperature, and enhance the accuracy of the SST estimation. The horizontally polarized brightness temperature of the LFMR could also be used in conjunction with the SSM/I to enhance the retrieval of surface wind speed and liquid water content.

The theoretical sensitivity studies indicate that a frequency in the 4 to 6 GHz region is optimal for the over-all retrieval of SST, and a frequency in the 8 to 10 GHz region is optimal for the retrieval of the SST of warm ocean water. The studies also indicate that both vertical and horizontal linear polarization are required for the retrieval of SST.

II.B. Analysis of Satellite Data

Theoretical models are versatile and convenient for various analyses and trade-off studies. Yet, their validity must be established through correspondence to reality. Two types of real data are available for the LFMR frequency selection. The first of these is satellite data. Among the satellite instruments that have been flown during the past decade, the only instrument which contains a multiple frequency passive microwave radiometer

containing frequencies in the required range of from 4 to about 10 GHz is the Scanning Multichannel Microwave Radiometer (SMMR). Both the SEASAT and the NIMBUS-7 satellites, launched in 1978, carried a SMMR. A number of serious problems complicate the proper interpretation of the SMMR data. However, careful selection of data and definition of retrieval algorithms have led to reasonable retrievals of the SST (1,5).

A study of the sensitivity of the two lowest frequencies (6.6, 10.7 GHz) of the SEASAT SMMR to SST and an analysis of the SST retrieval using these two frequencies was conducted by Frank Wentz of Remote Sensing Systems (RSS) (6). The total mission of SEASAT lasted 104 days; from June 28 to October 10, 1978. Wentz filtered the total SEASAT SMMR data set according to the following criteria: (1) only the middle two of the four 150 km SMMR brightness temperature cells for each scan are used in order to eliminate severe cross-track polarization error, (2) all data within 800 km of land are discarded to avoid side-lobe contamination problems, (3) only night-time data are used to avoid the Faraday rotation effect, sun glitter effect, sun entering the cold reference horn, and thermal gradients caused by heating effects which make the interpretation of day-time data unreliable, (4) only data from the second half of SEASAT's 3 month period were selected because the 18 GHz channel, which is used in the SST retrieval algorithm, showed a significant time dependent drift during the first half of the period. The climatological data used for comparison with the SEASAT SMMR SST retrievals (7,8) were compiled at NOAA.

Table 1 contains the most relevant results from the RSS study. The complete results of the RSS SMMR study are given in Appendix A. The slope between the brightness temperature and the climatological SST value is directly proportional to the cross correlation coefficient between the two variables. The brightness temperatures are sorted according to the corresponding climatological SST values into cold water, tepid water, and warm water categories. The slope at 10.7 GHz is higher than that at 6.6 GHz for warm water indicating higher sensitivity. The reverse is true for cold and tepid water. This result is in agreement with the theoretical results from subsection II.A. The SMMR brightness temperatures were also used to retrieve SST. The retrieval accuracies based upon the 6.6 GHz channels are superior to the retrievals based on the 10.7 GHz channels for all cases of liquid water content and surface wind speed (see Table 1). The 10.7 GHz retrievals are most accurate for tepid and warm water. This confirms the previous conclusions based on theoretical calculations that the frequency region of 4 to 6 GHz provides the most sensitive overall estimator of the SST except for warm water.

II.C Aircraft Measurements

During November-December 1982, NRL conducted a series of airborne radiometric measurements of SST. The instrument complement included the NASA/Langley Stepped Frequency Microwave Radiometer (SFMR) (9) and the NRL SSM/I simulator with channels at 19 H and V, 22 V, and 37 H and V mounted on a pallet aboard the NRL RP-3A aircraft. The pallet can be tilted to provide incidence angles from nadir to 53 degrees. The SFMR is vertically polarized and is electronically stepped over the range of 4 to 7.5 GHz. The frequencies chosen for data collection are 4.530, 4.994, 6.594, and 7.394 GHz centered on a bandpass of 50 MHz. A precision radiometric thermometer

TABLE 1

STATISTICS FROM THE N-ROSS SST STUDY USING
SEASAT SMMR AND CLIMATOLOGY

		SST RETRIEVAL* vs CLIMATOLOGY				BRIGHTNESS TEMPERATURE*** vs CLIMATOLOGY			
		SLOPE****		STD.DEV.**		SLOPE		STD. DEV.**	
		6.6 GHz	10.7 GHz	6.6 GHz	10.7 GHz	6.6 GHz	10.7 GHz	6.6 GHz	10.7 GHz
< 15°C	COLD WATER	1.0152	1.0432	1.85	2.37	0.3491	0.1996	2.95	3.59
15-25°C	TEPID WATER	0.8239	0.7352	1.40	1.63	0.4853	0.4065	1.96	2.41
> 25°C	WARM WATER	1.1269	1.1618	1.24	1.17	0.6379	0.9061	1.05	1.44
< 10 m gm/cm^2	CLEAR	0.9270	0.8874	1.51	1.89	0.4504	0.3668	4.15	4.82
10-25 m gm/cm^2	CLOUDY	0.8697	0.8065	1.78	2.14	0.3513	0.2461	4.65	5.50
25-200 m gm/cm^2	RAIN	0.8686	0.8201	1.77	2.24	0.3090	0.1984	5.06	5.94
< 7 m/s	LIGHT WIND	0.9330	0.8503	1.38	1.68	0.5641	0.5280	2.67	3.05
7-14 m/s	MEDIUM WIND	0.8980	0.8422	1.70	2.10	0.4946	0.4143	3.81	4.55
> 14 m/s	HIGH WIND	0.9487	0.9951	2.05	2.60	0.4633	0.3727	3.19	3.78

* SST RETRIEVALS ARE MADE USING 6.6 H, 6.6 V, (OR 10.7 H, 10.7 V), 18 V and 21 V SMMR CHANNELS.

** STANDARD DEVIATION OF THE DIFFERENCE BETWEEN EITHER THE SST RETRIEVALS OR THE T_B's, AND THE SST CLIMATOLOGY.

*** THE VERTICAL POLARIZED BRIGHTNESS TEMPERATURES ARE USED.

**** SLOPE OF THE REGRESSION LINE BETWEEN THE SST CLIMATOLOGY AND THE PARTICULAR VARIABLE.

(PRT-5) provides the surface truth measurements of the SST. Flights were conducted across the Gulf Stream, the continental shelf off the Norfolk, VA coast, Gulf of St. Lawrence, the Labrador Sea, and Frobischer Bay covering a SST range from 2 to 25 C. The pallet angle was set at 0, 10, 20, 30, 40 and 50 degrees. The SFMR instrument failed several times during the mission and the mechanism which tilts the pallet locked at nadir several times due to the extremely cold conditions in Labrador. As a result, very little of the SFMR data are actually usable for this study. The brightness temperatures at 4.530 GHz for the pallet angles of 0 and 40 degrees are shown in Figures 5 and 6 as functions of sea surface temperature. Even though the data were collected on different days, over different locations, and under different weather conditions, the 4.530 GHz frequency is shown to be significantly sensitive to SST. The slope of the regression line in the Figure 6 for the 40° look angle is greater than that of the nadir looking case in Figure 5. These slopes are somewhat greater than those from the SEASAT SMMR statistics (see Table 1) or the theoretical studies (see Figure 1). Even though the extent of the aircraft data is very limited, the results are in general agreement with the theoretical calculations and substantiate the theoretical approach.

II.D Retrieval Accuracy

The confirmation of the theoretical sensitivity studies by the satellite and aircraft measurement results provides the practical basis for detailed theoretical retrieval and trade-off studies. Several independently developed geophysical models and retrieval algorithms are available to be used in parallel to assure consistency and reliability of the study results. Alex Stogryn of the Aerojet and Electro Systems (AES) and Gene Poe* of the Hughes Aircraft Company (HAC) have conducted extensive investigations in the field of microwave remote sensing (e.g. 10, 11, 12, 13, 14) and have independently developed geophysical models and retrieval algorithms applicable to the study of the microwave radiometric determination of SST. Their models share in common, parts of the physical relationships, as of course they must; however, the retrieval methods and the data base employed are sufficiently different so as to render the models independent for practical purposes. Stogryn and Poe volunteered to join NRL in an independent SST retrieval study. A common set of environmental and experimental parameters and ranges were agreed upon and are given in Table 2.

The range of environmental condition chosen covers all but the most extreme conditions likely to be encountered. The frequency pairs were chosen to contain a lower frequency from the optimal region of 4 to 6 GHz and a higher frequency which will have greater sensitivity in warmer ocean waters and provide greater spatial resolution.

The effects of instrumental noise, ΔT, and of using SSM/I environmental products in the SST retrieval are of particular interest. The SSM/I is expected to provide estimates of wind speed, water vapor, and liquid water at accuracies of 2 m/sec, 0.2 gm/cm^2, and 0.01 gm/cm^2, respectively.

Poe performed retrievals for instrumental noise, ΔT, temperatures of 0.0 and 0.25 K testing all the frequencies and frequency combinations using

*Gene Poe has since joined Aerojet Electro Systems.

SSM/I products. His results are given in Figures 7 and 8 and indicate that it is possible to achieve the operational requirement of 1 C for SST, for a noise uncertainty of 0.25 K or less, using a dual-polarized single-frequency system at a frequency of 6.5 GHz or less. The results also indicate that it is not possible to reach the required accuracy using either a 10.7 or an 8.6 GHz system, even when the SSM/I products are used in the retrieval. The retrievals from a dual-frequency system perform consistently and significantly better than those of the single-frequency system.

TABLE 2

1. Environmental Conditions

SST (C)	-2 to 30
Wind Speed (m/sec)	2 to 17
Salinity (PPT)	33 to 37
Columnar density of water vapor (gm/cm^2)	0.6 to 6.0
Columnar density of liquid water (gm/cm^2)	0.0 to 0.08
Air temperature (C)	0 to 32

2. Frequencies for consideration (both polarizations)

   4.3, 5.1, 6.5, 8.6, 10.7 GHz and (4.3, 8.6 GHz), (5.1, 10.7 GHz) combinations

3. Instrument noise ΔT

   0.0, 0.25, 0.5 and 1.0 K

Stogryn's retrieval results are depicted in Figures 9 through 11. The results in Figure 9 confirm the conclusion from Poe's study that the retrievals based on either 8.6 or 10.7 GHz alone are not adequate to meet the operational requirement even using SSM/I products. For an instrumental noise of 0.5 K or less, the lower frequencies may be used alone to retrieve SST. The RMS retrieval error values vary somewhat between Stogryn's and Poe's models, but the general characteristics and trends agree very well.

Stogryn examined the two-frequency combinations with and without SSM/I products. The retrievals for the 4.3, 8.6 GHz combination are shown in Figure 10. Retrievals using only the single 4.3 GHz frequency are also included in this figure to provide a reference for comparison with the dual-frequency system. The additional frequency improves the retrieval results much more significantly than including the SSM/I products. When two

frequencies are used, the inclusion of the SSM/I products adds only minute improvement, implying that the SSM/I products are not necessary for a dual-frequency LFMR. This would relieve constraints on the spacecraft interface design imposed by requiring common lines of sight for both the LFMR and the SSM/I. Another benefit of using a dual-frequency system is redundancy in case of partial failure, such as the loss of one channel. The dual-frequency system also provides higher accuracy, and the higher frequency channels provide better surface resolution in warm ocean water regions.

Similar retrieval results for the 5.1, 10.7 GHz combination are presented in Figure 11. The same conclusions, as derived from the 4.3, 8.6 GHz system, are supported by this set of simulations. The inclusion of the SSM/I products only marginally improves the retrievals when a two-frequency configuration is used for the LFMR and a dual-frequency system is far superior to a single-frequency system. The 4.3, 8.6 GHz combination appears to be slightly better than the 5.2, 10.7 GHz system in retrieval accuracy. But both of these combinations are adequate to meet the operational requirements if a system noise of about 0.5 K or less can be achieved.

NRL performed the simulations in the same fashion as Stogryn. The results are shown in Figures 12 through 14. A difference between the two sets of results is that the climatology used to develop the NRL retrieval algorithm is assumed to describe the environment perfectly. Under such conditions, the retrieval contains no error when the measurement is perfect, i.e., when there is no instrumental noise. Stogryn's model employs different sets of actual radiosondes for model development and for retrieval. The difference between the two sets of radiosondes imposes a modelling error not included in the NRL approach. Therefore, the NRL results differ from Stogryn's for very small system noises. The Stogryn and NRL results are in agreement for system noises of about 0.5 K or greater. If a modelling error is introduced into the NRL retrieval with the same magnitude as is implied in Stogryn's results at zero system noise, the two approaches yield nearly identical results. The NRL simulation results are in agreement with those of Poe and Stogryn and suggest the use of a dual-frequency, dual-polarized system for the LFMR.

Although theoretical studies may be questioned on the basis of how well they represent nature and the real world, the excellent agreement among the three different retrieval studies and the agreement of the theoretical model with the aircraft and satellite measurements encourage confidence in the conclusions derived from the theoretical studies.

III. RFI, FARADAY ROTATION, SUN GLINT, AND ANTENNA DISH SIZE CONSIDERATIONS

The sensitivity and retrieval simulation studies suggest that either the 4.3, 8.6 GHz or the 5.1, 10.7 GHz combination is a reasonable choice for the LFMR. The exact frequencies are not critical and depend upon further considerations of the operational requirement for surface resolution, antenna size, antenna weight, and LFMR power consumption limitations. In addition, radio frequency interference (RFI) must be considered in the selection of the exact frequencies. Faraday rotation caused by the earth's magnetic field in the ionosphere is known to affect low frequencies in the

microwave range, and sun glint is also a significant source of error for microwave remote sensing. These matters are considered in the following sections.

III.A RFI

One of the problems encountered by the SEASAT and the NIMBUS-7 SMMR instruments was RFI, particularly at 6.6 GHz. A survey of potential RFI sources germane to satellite-borne microwave radiometers was performed at NRL (15) in connection with design studies for LAMMR. The results for the 4 to 6 GHz region were compiled (16) and are presented in Figure 15. There is a band at least 200 MHz wide around 4.3 GHz which is relatively emitter free. Similarly, the 400 MHz wide band centered around 5.2 GHz has relatively few emitters. Based on this information, tentative frequency combination for consideration are 4.3, 8.6 GHz and 5.2, 10.4 GHz, with the higher frequency in each pair arbitrarily chosen an octave above the lower frequencies. The 5.2, 10.4 GHz combination is to be preferred on the basis of providing higher surface resolution if other considerations allow it.

A more significant RFI parameter is the total power of the radio emitters rather than their number. The studies (15, 16) did not address the power emitted and did not survey the whole frequency range of present interest. Further RFI investigations are clearly necessary before a final frequency selection for the LFMR is made.

III.B Faraday Rotation

The plane of polarization of microwave radiation propagating upward through the earth's ionosphere is rotated by an angle, $\Delta\theta$, by Faraday rotation (17). The amount of rotation depends upon the magnitude and orientation, with respect to the direction of propagation, of the earth's magnetic field and the density of electrons along the propagation path. It is given by,

$$\Delta\theta = \frac{2.36 \times 10^4}{f^2} \int NH \cos\phi \, dr \qquad (1)$$

where f is the observational frequency in Hertz, H is the earth's magnetic field in Gauss, N is the electron number density in cm^{-3}, and dr is an element of length along the path of integration through the ionosphere in cm (18). Ionospheric Faraday rotation determined from equation (1) using the mean values of 0.47 Gauss for H, 45^o for ϕ and 3.8×10^{13} cm^{-2} for the integral of N along the propagation path is given in Figure 16 as a function of frequency. Rotation can be as much as three or more times the values given in Figure 16 during the solar sunspot maximum and for extreme values of H $\cos\phi$. It should be noted that N-ROSS is scheduled for launch near sunspot maximum. Thus Faraday rotations of several degrees may be expected at the lower frequencies of interest.

The rotation of the plane of polarization by ionospheric Faraday rotation, if uncorrected, will result in an error in the measured vertical and horizontal linearly polarized brightness temperatures of ΔT_B given by

$$\Delta T_B = (T_{BV} - T_{BH}) \sin (2\theta + \Delta\theta) \sin \Delta\theta. \qquad (2)$$

Here T_{BV} and T_{BH} are the true vertical and horizontal brightness temperatures of the radiation at the earth's surface, θ is the angular orientation that the plane of reception of the receiving antenna at the satellite makes with respect to the surface vertical, and $\Delta\theta$ is the Faraday rotation. If θ is large compared to $\Delta\theta$

$$\Delta T_B \simeq (T_{BV} - T_{BH}) \sin 2\theta \sin \Delta\theta, \qquad \theta >> \Delta\theta, \qquad (3)$$

then ΔT_B is proportional to sin $\Delta\theta$. This is the case with SMMR where the plane of polarization rotates with scan angle and θ can be as large as 25°. If θ can be held constant at 0°, independent of scan angle, then

$$\Delta T_B = (T_{BV} - T_{BH}) \sin^2 \Delta\theta, \qquad \theta = 0, \qquad (4)$$

and ΔT_B is proportional to $\sin^2\Delta\theta$. This can be a very large difference. For example for $T_{BV} - T_{BH} = 100$ K, $\theta = 25^\circ$, and $\Delta\theta = 3^\circ$ equation 3 gives a brightness temperature error of 4 K whereas an error of only 1/4 K results from equation (4) when $\theta = 0$. Therefore, an important design consideration is to maintain the reception plane of polarization aligned with vertical at the earth's surface independent of scan angle. The expected error, under the mean conditions assumed above, calculated using equation (4) is also plotted in Figure 16 using a value of 100 K for $T_{BV} - T_{BV}$ which is an upper limit even at 15 GHz. For example, at 4.3 GHz, the error is approximately 0.03 K and may be as large as 0.1 K under severe ionospheric conditions. The error decreases quickly with increasing frequency, and normally, will not be important and can be ignored. If necessary, a relatively simple correction can be made to remove the bulk of the effect since Faraday rotation is systematic and well understood. Only if the plane of polarization rotates with scan angle will Faraday rotation be a problem.

III.C Sun Glint

Sun glint is caused by the specular reflection of solar radiation from the sea surface. The sun is very intense at microwave frequencies, especially during periods of high sun spot activity when it can have brightness temperatures as high as 40,000 K at 10 GHz and more then 200,000 K at 5 GHz. Therefore, it can cause a large contribution to the observed brightness temperature when the specular point falls within the footprint of the observing radiometer. The brightness temperature error caused by sun glint is a function of angle relative to the specular angle and the surface roughness of the sea which is primarily a function of wind speed. Studies have been performed (19, 20) for the purposes of defining a cone angle about the direction where sun glint presents a problem in environmental parameter retrievals. Consideration has also been given to the possibility of generating a correction algorithm. These studies indicate sun glint effects can cause brightness temperature increases in excess of 1 K for angles within $\pm 20^\circ$ of bistatic for the SMMR 6.6 GHz channel. Unfortunately, the

sun glint problems cannot be avoided nor be obviated by system design or frequency selection. Fortunately, sun glint problems are minimized by the sun synchronous early morning orbit planned for N-ROSS. The 98.1° retrograde N-ROSS orbit is shown in Figure 17 with solar positions at summer and winter solstice and the equinoxes indicated for both a 7:15 a.m. and an 8:15 a.m. equatorial crossing. The limit of the LFMR scan is shown by the small circle labeled "swath edge". There will be no specular solar reflection for any sun position within this circle. However, under rough surface conditions scattered solar radiation will be received from directions considerably away from the specular direction (19, 20). Thus, sun glint will be a problem at some scan angles over some portions of the orbit, primarily near the swath edge in the summer. Criteria for its detection and elimination must be determined in a way similar to that done for the SMMR (19, 20) experiment. This problem will have to be addressed in the processing software rather than instrument design.

III.D Antenna Dish Size

The primary factors for the determination of antenna dish size are the Navy's operational requirements for surface resolution, the spacecraft volume and weight allowances for the LFMR instrument, and the state of the art in antenna design. According to the spacecraft configuration work force (RCA) and the antenna industry, the antenna for LFMR must be significantly below 10 meters in diameter. The Navy's operational target requirement for surface resolution is 10 kms and the acceptable resoultion is 25 kms.

The surface resolution size of the LFMR depends on the slant range, ℓ, which is a function of satellite height and the incidence angle, I_o, of the LFMR, as well as the wavelength, λ, and the antenna aperture diameter, d. For a conically scanning instrument, such as the SSM/I, the half-power footprint is approximately elliptical with the along track dimension, D_a, and cross track dimension, D_c given by

$$D_a = \frac{1.2\lambda\ell}{d \cos I_o} \quad \text{and} \quad D_c = \frac{1.2\lambda\ell}{d}. \qquad (5)$$

Assuming that the LFMR scan geometry is the same as the SSM/I, the along track and cross track surface resolutions for a number of antenna apertures are presented in Figures 18 and 19.

The target requirement of 10 km cannot be met at the lower frequencies of the 4.3, 8.6 GHz and 5.2, 10.4 GHz pairs under consideration unless the antenna aperture is significantly greater than 10 meters. The acceptable requirement of 25 kms is met in both along and cross track directions at 5.2, 8.6, and 10.4 GHz by a 6-meter diameter antenna. A 6-meter antenna will also meet the acceptable requirement of 25 kms at 4.3 GHz in the cross track direction and will meet the target resolution requirement of 10 kms along and cross track at the two higher frequencies. Furthermore, a smaller dish of 3.6 meters would meet the acceptable resolution requirement at 5.2, 8.6, and 10.4 GHz cross track but only at the two higher frequencies along track. At present it appears possible to build a 6-meter diameter antenna which is within the weight specification and can be folded and stowed in the

volume available in the launch shroud. Therefore, a 6 meters target size for the LFMR antenna is adopted. The 5.2, 10.4 GHz pair of frequencies is preferred to the 4.3, 8.6 GHz pair because they allow the resolution requirement to be met with the 6.0 m antenna in both the along track and the cross track dimensions and with the 3.6 m antenna in the cross track direction.

IV. BASELINE MODEL OF THE LFMR

The sensitivity and retrieval accuracy studies described in Section II indicate that the 4.3, 8.6 GHz frequency combination may be marginally better for SST retrieval than the 5.2, 10.4 GHz pair. However, any possible slight improvement in SST retrieval accuracy obtainable with the low frequency combination is negligible compared to the 21 percent increase in surface resolution provided by the higher frequency combination. Since both accuracy and resolution are important considerations, the 5.2, 10.4 GHz combination will better meet the operational requirement than will the 4.3, 8.6 GHz pair. Further, uncertainities in the measured brightness temperature caused by Faraday rotation, as described in Section III.B, will be about half as large for the higher-frequency combination and, since solar intensity decreases with increasing frequency, sun glint problems will also be somewhat smaller. For these reasons the frequencies of 5.2 and 10.4 GHz are selected over 4.3 and 8.6 GHz for the baseline instrument.

An incidence angle near 50° is required to enable corrections for marine wind speed and a conical scan geometry, similar to that of the SSM/I (21), is indicated for the same reasons that led to its use for SMMR, SSM/I, and LAMMR. The adoption of a scan geometry identical to the SSM/I will facilitate data comparisons between the two instruments and will ease the development of algorithms using different combinations of channels from both systems. Further it will enable a common format and use much of the same software for data display, handling, and distribution. This scan geometry is shown in Figure 20. It is a conical scan at a 53.1° incidence angle. Measurements of the scene are obtained over a 102.4° scan angle centered on the satellite ground track. A scan period of 1.9 seconds leads to a 12.5 km spacing between successive scans for a satellite altitude of 833 km.

A minimum antenna size of 3.6 m diameter is required to obtain a 25 km half-power footprint in the cross track direction but only provides a 42 km footprint in the along track direction at 5.2 GHz. The surface resolution at 10.4 GHz is, of course, one half of these values. If the output of the radiometers is sampled each 12.5 km along the scan direction, the same as the along track spacing, the 5.2 GHz channels will be Nyquist sampled, i.e. sampled at intervals of one half or less of the antenna surface resolution, but the 10.4 GHz channels will not be. Nyquist sampling is very important to prevent aliasing and allow the full use of the antenna resolution for locating and mapping thermal fronts and eddies, ice edges, and other surface features. This results in 128 samples per scan and requires a 118 GHz low pass filter at the radiometer output prior to sampling.

System temperatures of 250 K are obtainable with FET amplifiers at 5 and 10 GHz. If a calibration scheme similar to that used for the SSM/I can be designed for the LFMR, a total power radiometer can be used. Bandwidths

of 300 MHz and 500 MHz are achievable at 5 and 10 GHz and should be compatible with RFI considerations. Ocean scene temperatures will be about 130 K and 150 K leading to RMS noises of 0.34 K and 0.27 K per sample at 5.2 and 10.4 GHz. Sampling both polarizations, with 12-bit precision, will result in a 1.6 kb/s data rate at each frequency. Assuming about 0.5 kb/s for scan position, reference temperatures, and other instruments condition and performance data requires a total data rate of 3.7 kb/s. All of these considerations of sampling, resolution, noise, and data rate for a 3.6 m antenna are summarized in Figure 21.

In order to obtain Nyquist sampling at 10.4 GHz as well as at 5.2 GHz a second dual polarized 10.4 GHz system must be added. This would be a second feed, offset in both the along and cross track directions, so as to provide the footprints shown in Figure 22. This would provide two series of 10.4 GHz samples spaced by 6.2 km in the along track direction each scan. Sampling each 6.2 km along the scan direction to provide a 6.2 x 6.2 km grid would lead to an increased sample noise of 0.39 K and quadruple the data rate for 10.4 GHz. The overall data rate would increase to 8.6 kb/s.

In order to obtain 25 km resolution in the along track direction at 5.2 GHz, a 5.9 m diameter antenna is required. This would provide 15 x 25 km resolution at 5.2 GHz and 8 x 13 km resolution at 10.4 GHz. The resolution at 10.4 GHz with a 5.9 m antenna is about 10 percent better than the SSM/I at 85.5 GHz. Samples at 7.5 km cross track are required for Nyquist sampling at 5.2 GHz. The resultant sampling, noise, and data rates are given in Figure 23. A second offset feed and dual polarized radiometric system must be added to achieve Nyquist sampling at 10.4 GHz. Samples will be obtained on a 3.8 x 3.8 km grid. This situation is summarized in Figure 24. It is still possible to meet the RMS noise requirement of 0.5 K. The overall data rate is 14.0 kb/s.

The 5.9 m antenna, six-channel, Nyquist sampled system meets the operational requirement in both accuracy and resolution. Since the major expense and weight of the system is required by the antenna, the addition of two-dual polarized radiometers and feeds at 10.4 GHz to a minimum 5.2 GHz system will only marginally increase the weight and power requirements, and the data rate of 14 kb/s is modest. The dual-frequency, dual-polarized, six-channel system provides greater accuracy over a larger range of SST, better surface resolution in warm ocean water regions, a stand alone system independent of the SSM/I, and redundancy in the event of partial system failure.

Nyquist sampling in both along and cross track directions will allow maximum use of the antenna resolution in mapping surface features. It should be noted the data can always be smoothed in post processing to decrease the RMS sample noise and increase retrieval accuracy to the same reduced surface resolution as would have been obtained originally if the data had not been Nyquist sampled. The reverse is not possible. If the scene is not Nyquist sampled, no post processing will restore the surface features to the maximum resolution allowed by the antenna.

The baseline system is given in Table 3. The weight, volume, and power requirements given for the antenna and radiometer were obtained from discussions with Harris Corporation and extrapolations from SMMR, SSM/I, and LAMMR.

TABLE 3

BASELINE SYSTEM

- Daul Frequency - 5.2 and 10.4 GHz
- Dual Polarization - horizontal and vertical linear polarization
- 45° Conical Scan (53.1° incidence angle at earth's surface)
- 1.9 second period
- 102.4° scan width

- Antenna - 5.9 m diameter
  - 70 lbs maximum weight
  - 22 FT^3 stowed volume
  - 20 watts power
  - Pointing accuracy $\pm 0.1^{\circ}$; precision $\pm 0.02^{\circ}$

- Resolution - 15 x 25 km-5.2 GHz
  - 8 x 13 km-10.4 GHz

- Radiometer - Total Power
  - Externally calibrated
  - Bandwidth 300 MHz 5.2 GHz
    500 MHz 10.4 GHz
  - ΔT noise 0.44 K 5.2 GHz
    0.50 K 10.4 GHz
  - 24 lbs weight
  - 24 watts power
  - six channel (H, V 5.2 GHz; 2H,2V 10.4 GHz)
  - Nyquist sampled
  - 14.0 kb/s data rate

- Orbit 833 km altitude
  98.7 inclination (polar orbit)
  DMSP constellation
  3 years mission life

Acknowledgments

We gratefully acknowledge the efforts of Gene A. Poe of the Hughes Aircraft Company and Alex Stogryn of Aerojet Electro Systems who independently conducted and made available to us the theoretical sensitivity studies presented in Section II.A. In addition we greatly benefited from numerous discussions with each of them. Their ideas, analyses, and critiques have significantly enhanced this study. Any shortcomings are ours alone. We also appreciate the orbit calculations John Eisele of the Naval Research Laboratory provided us, which are shown in Figure 17. Frank Wentz's study using SEASAT SMMR and SASS data as shown in Section II.B and Appendix A was also most valuable.

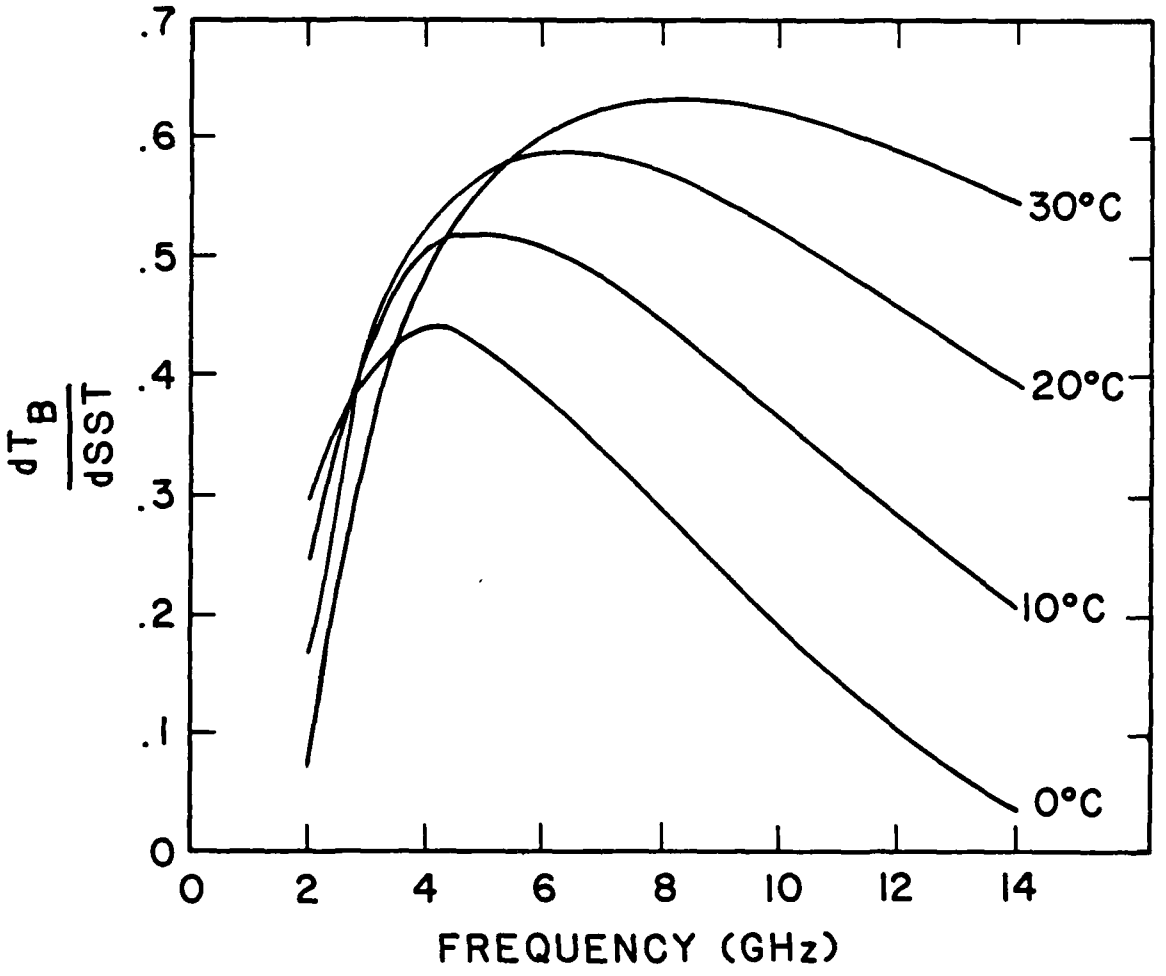

Figure 1 Sensitivity of brightness temperature to SST as function of frequency

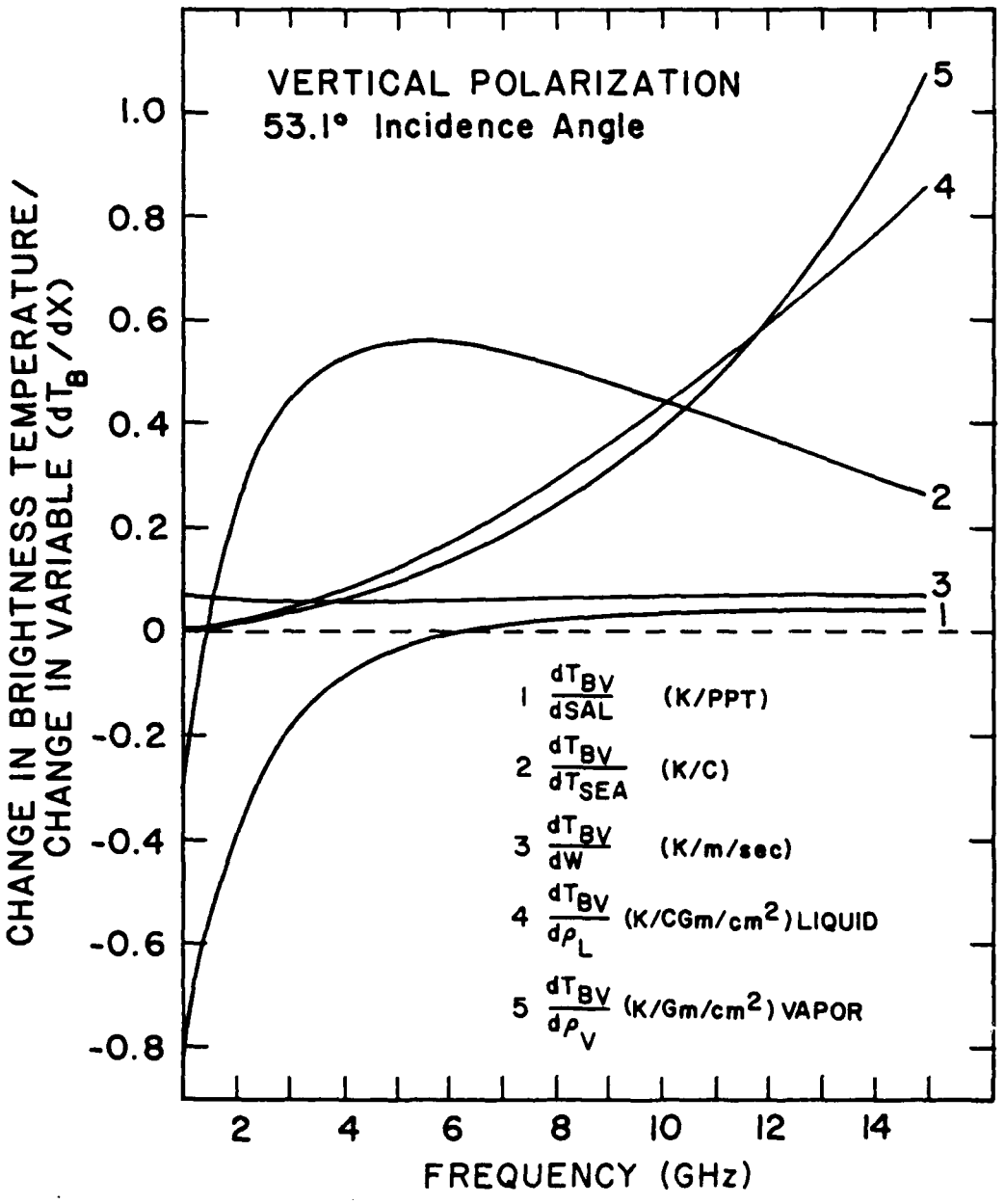

Figure 2 Change in brightness temperature w.r.t. change in environmental parameters

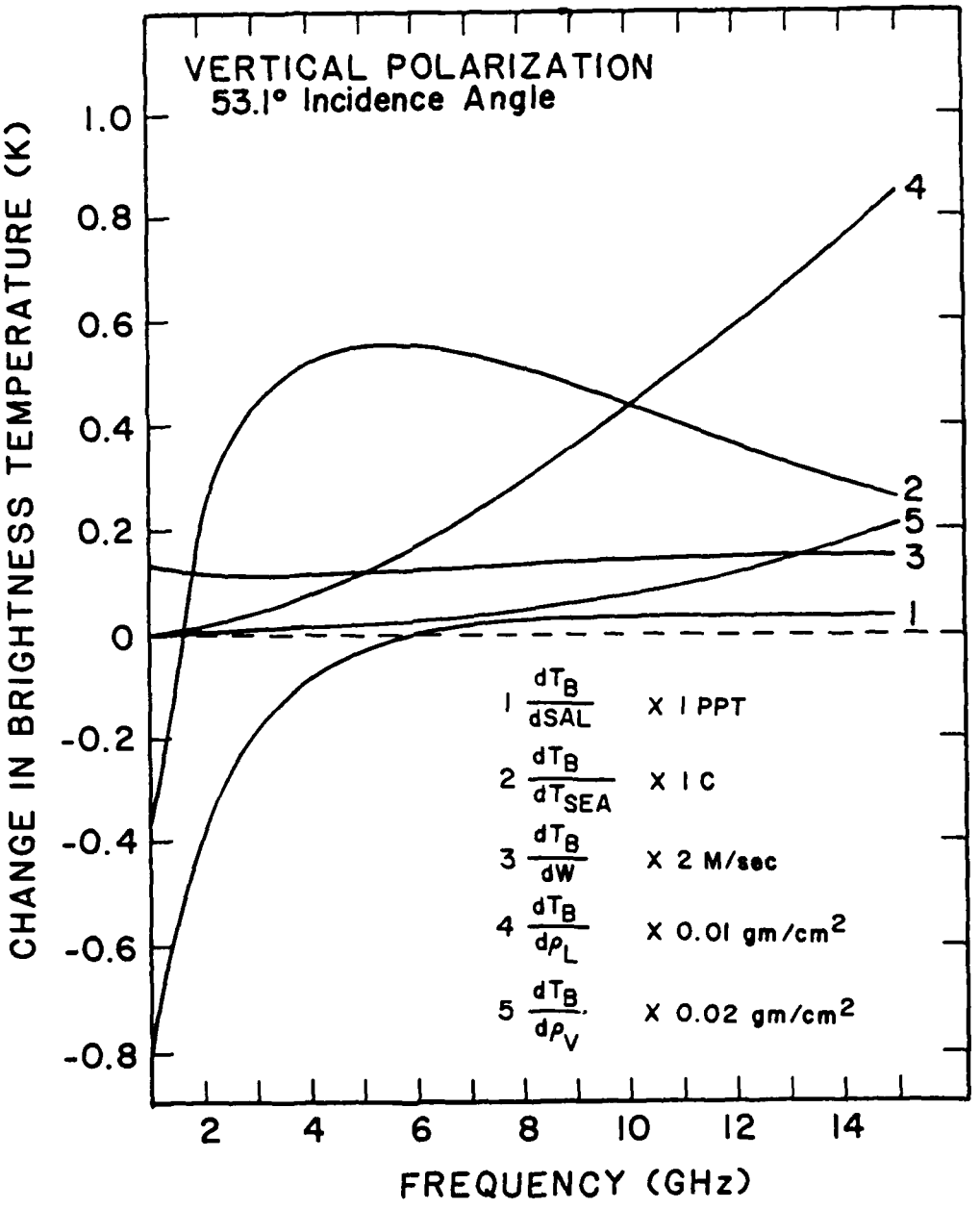

Figure 3 Change in vertically polarized brightness temperature as function of frequency

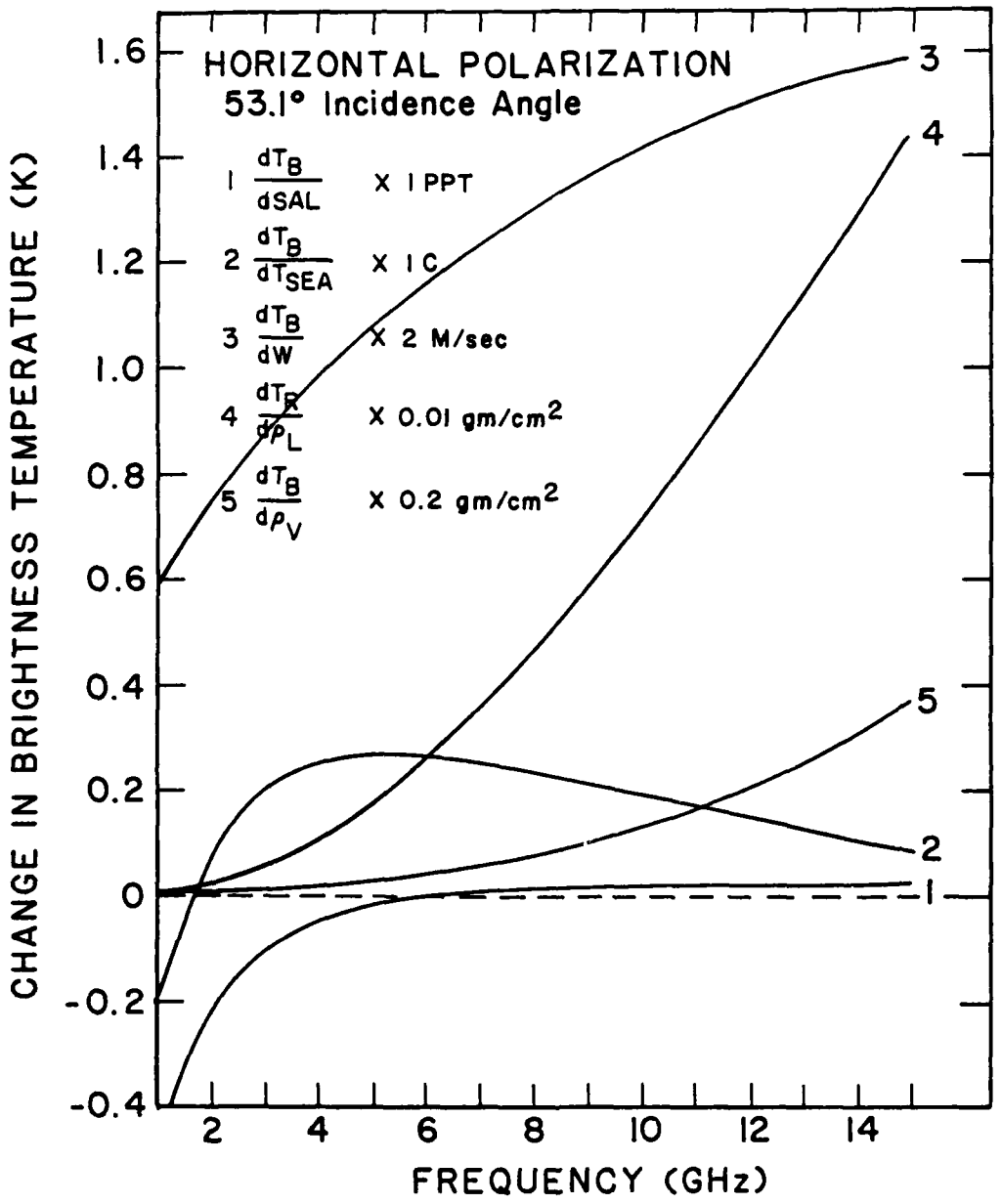

Figure 4 Change in horizontally polarized brightness temperature as function of frequency

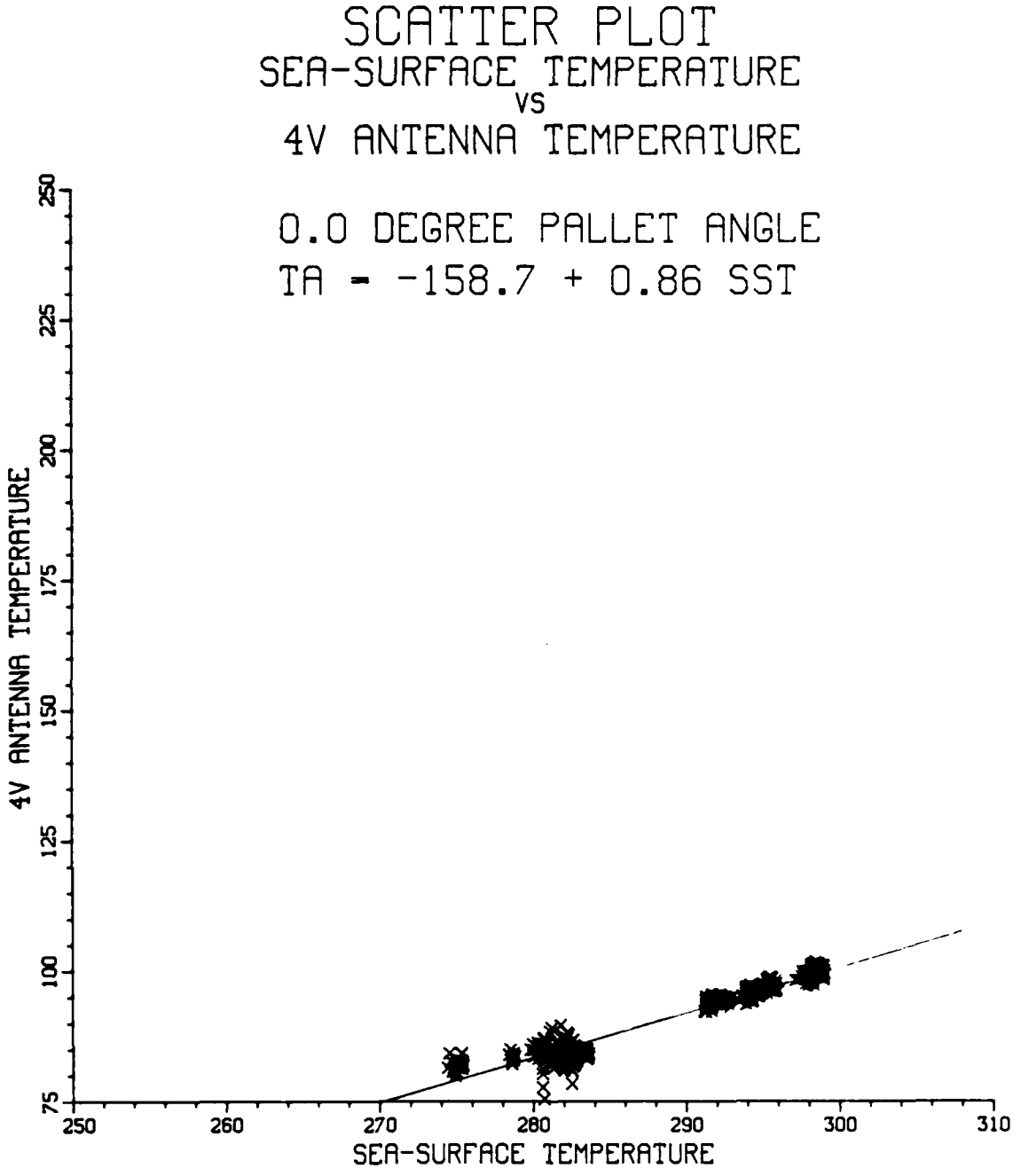

Figure 5 SFMR 4.5 GHz antenna temperature vs SST at 0° pallet angle

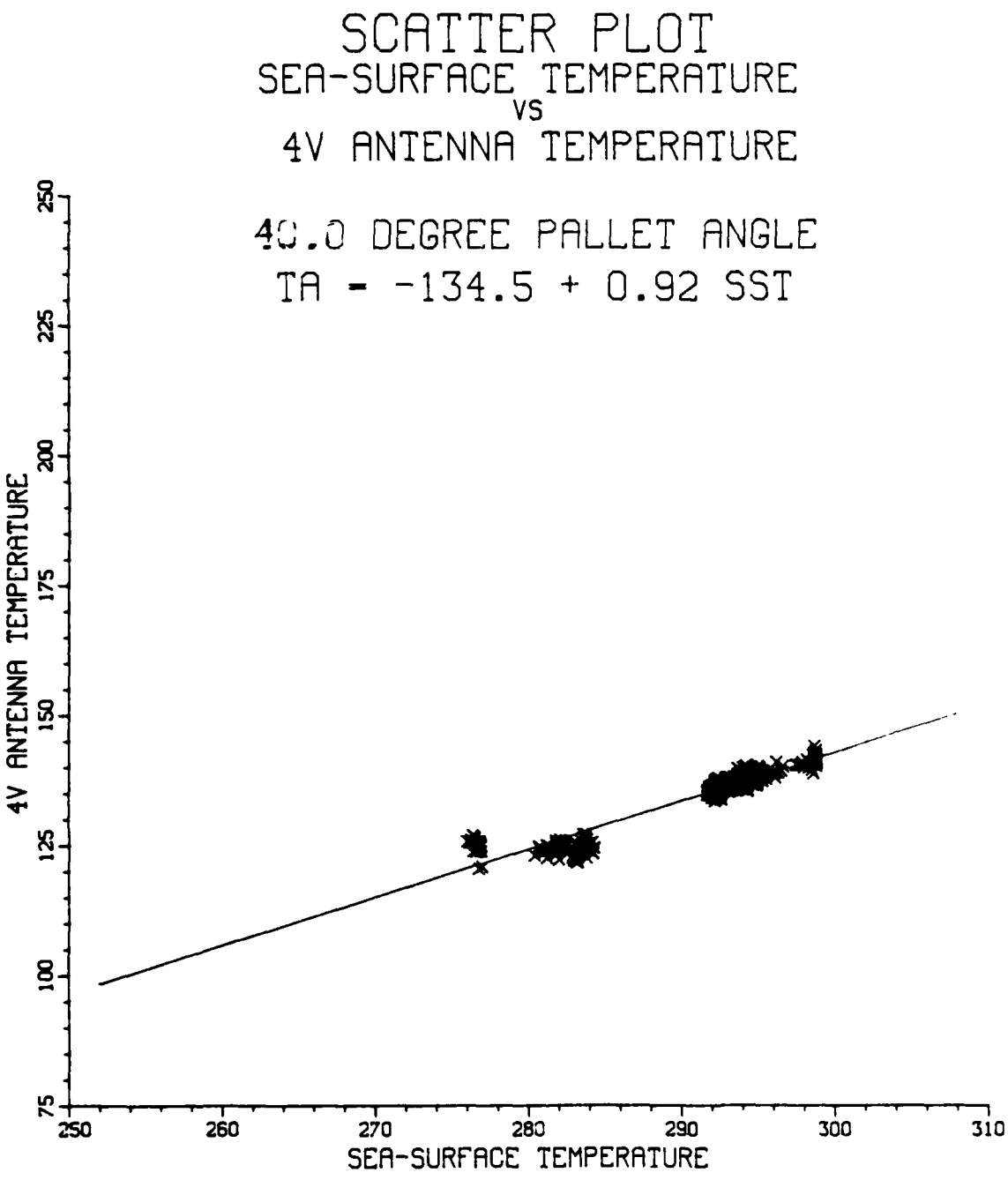

Figure 6 SFMR 4.5 GHz antenna temperature vs SST at 40° pallet angle

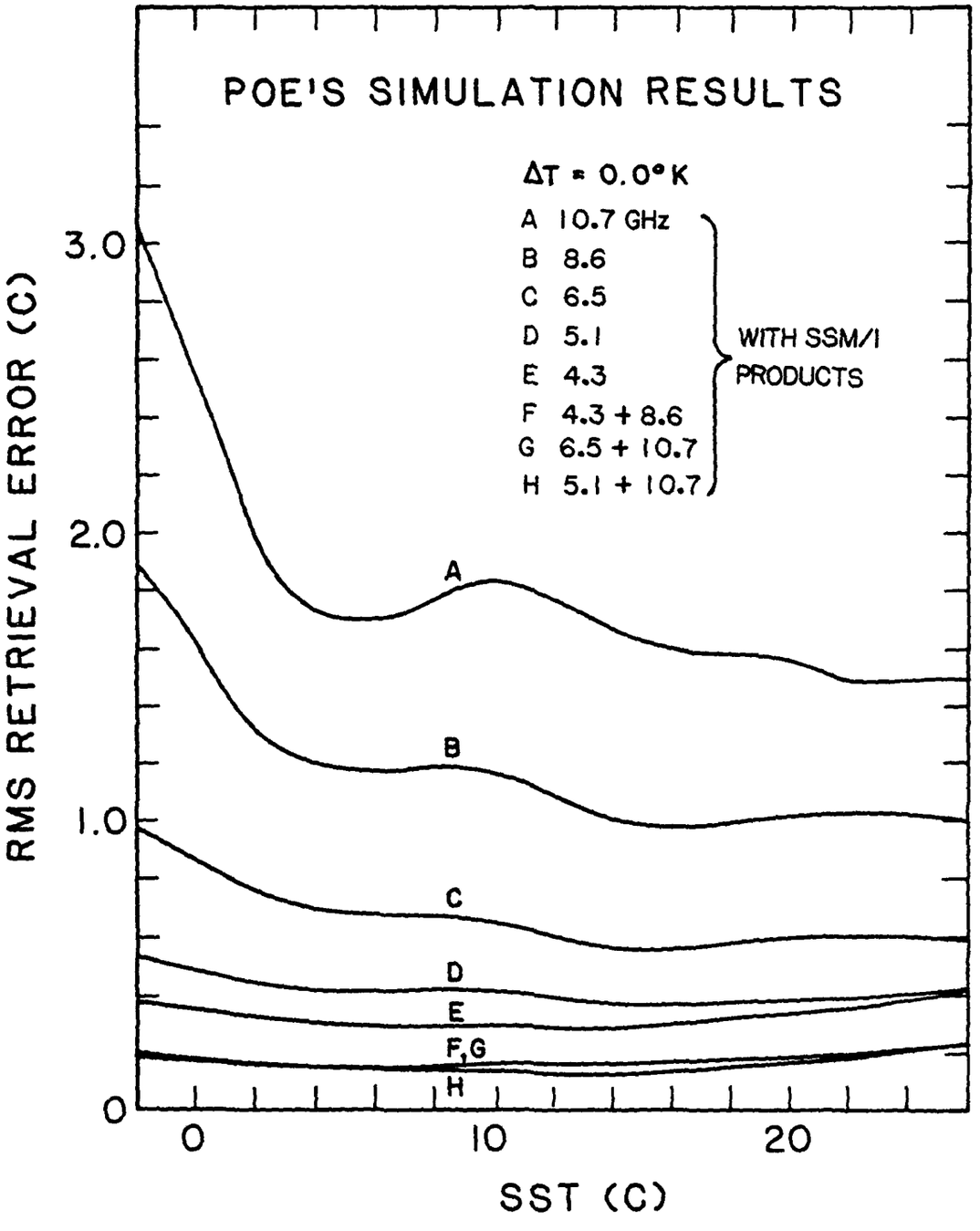

Figure 7 Poe's retrieval results for ΔT = 0.0 K

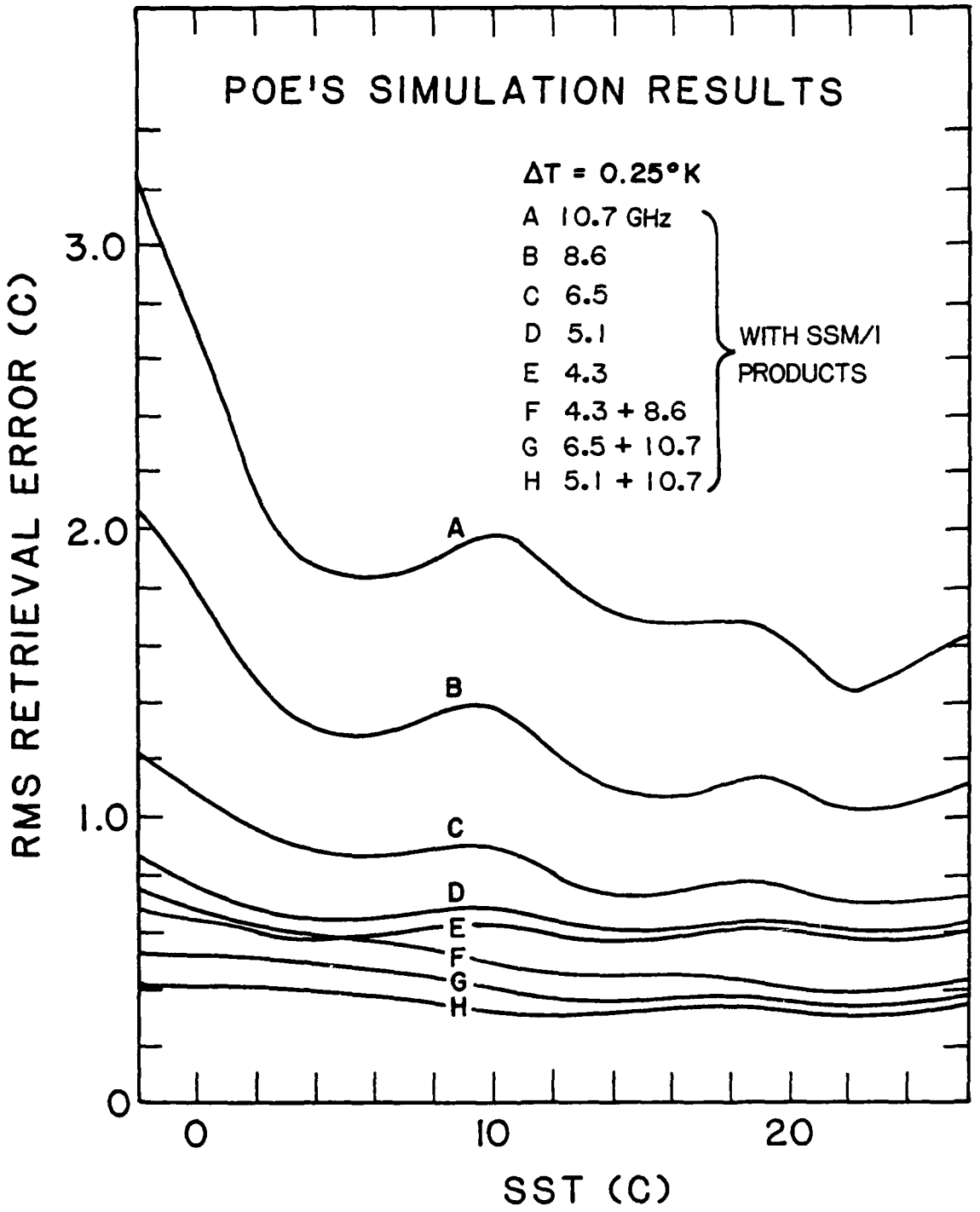

Figure 8 Poe's retrieval results for ΔT = 0.25 K

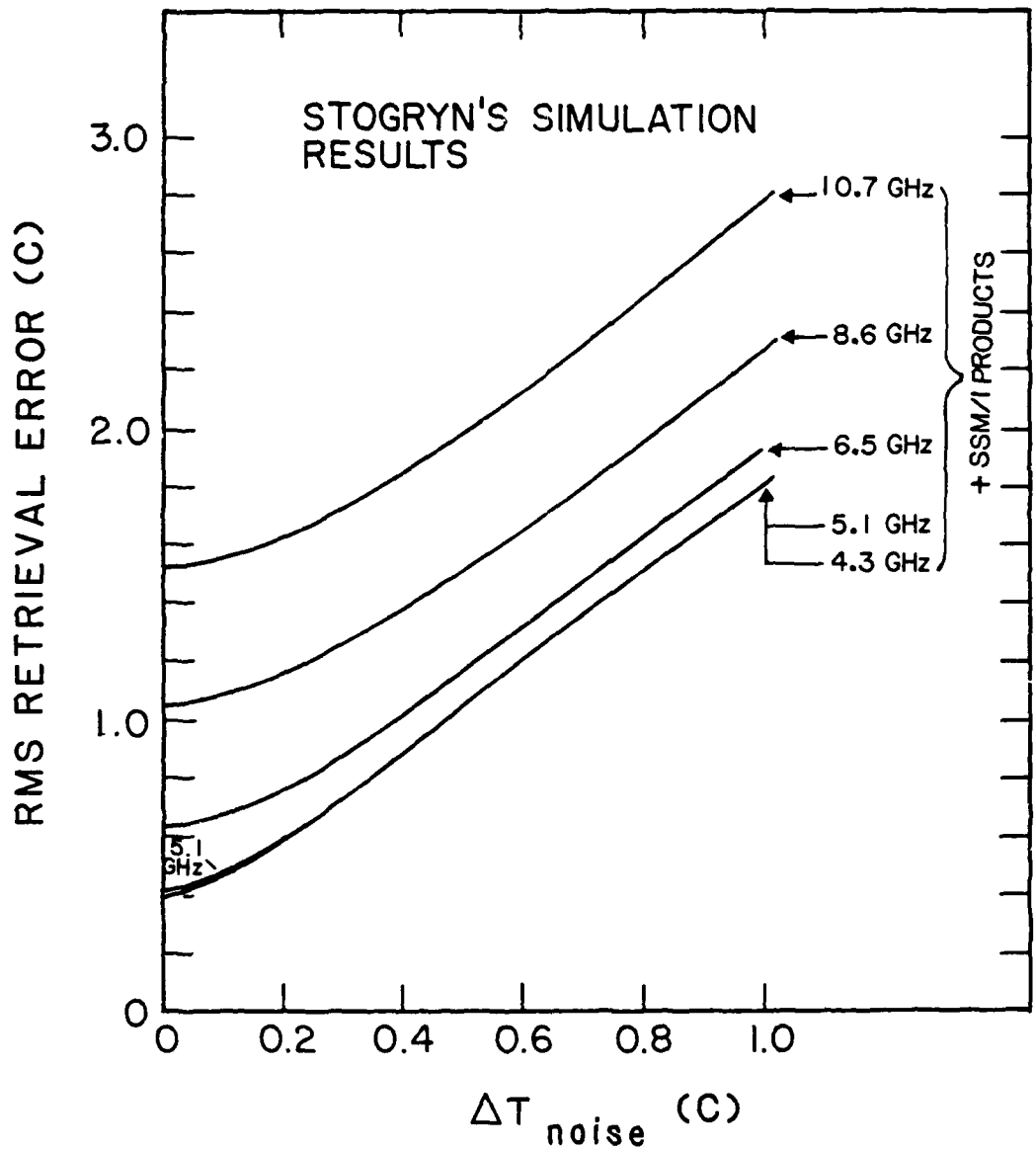

Figure 9 Stogryn's retrieval results for single frequencies

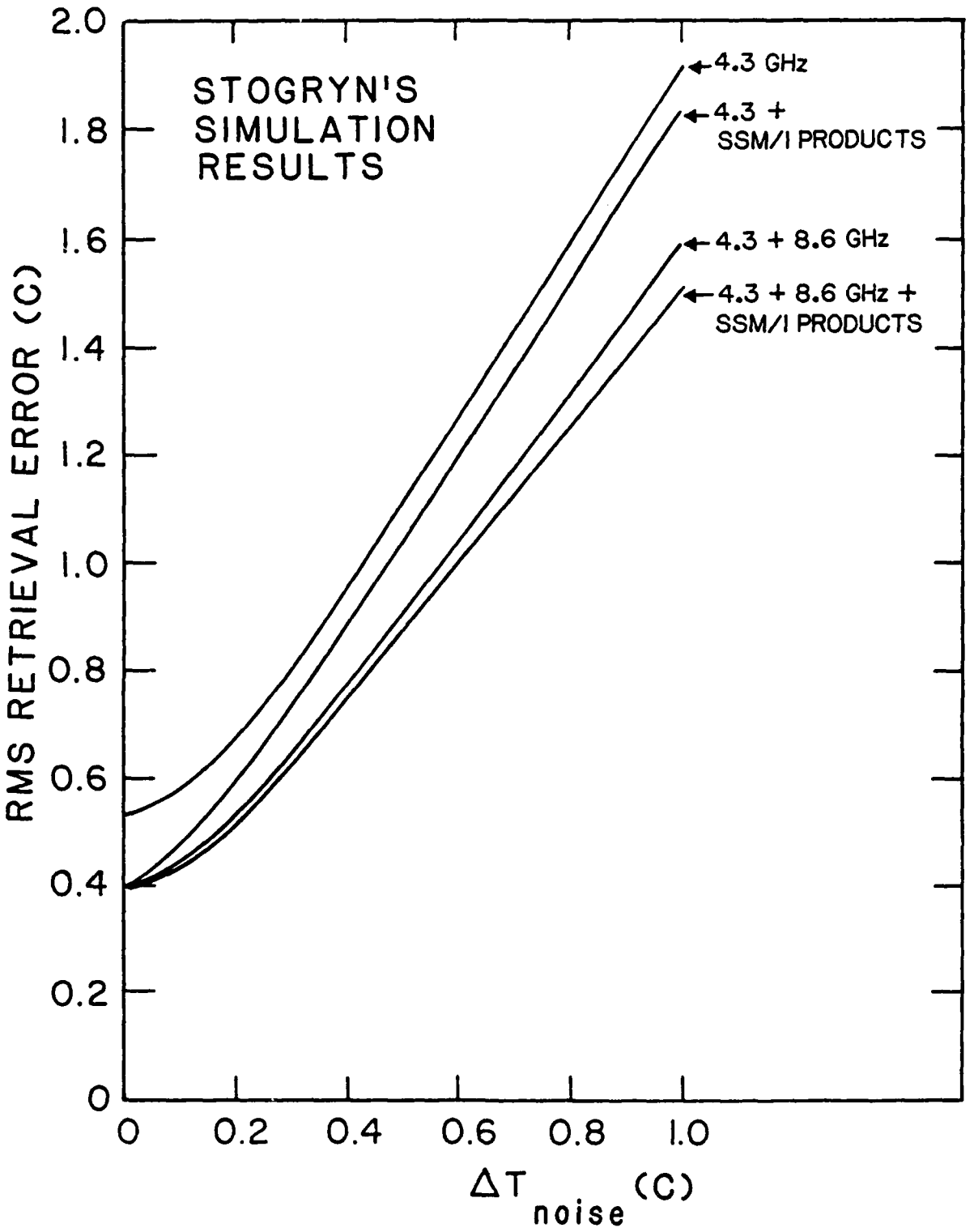

Figure 10 Stogryn's retrieval results for 4.3 GHz and 4.3, 8.6 GHz combination

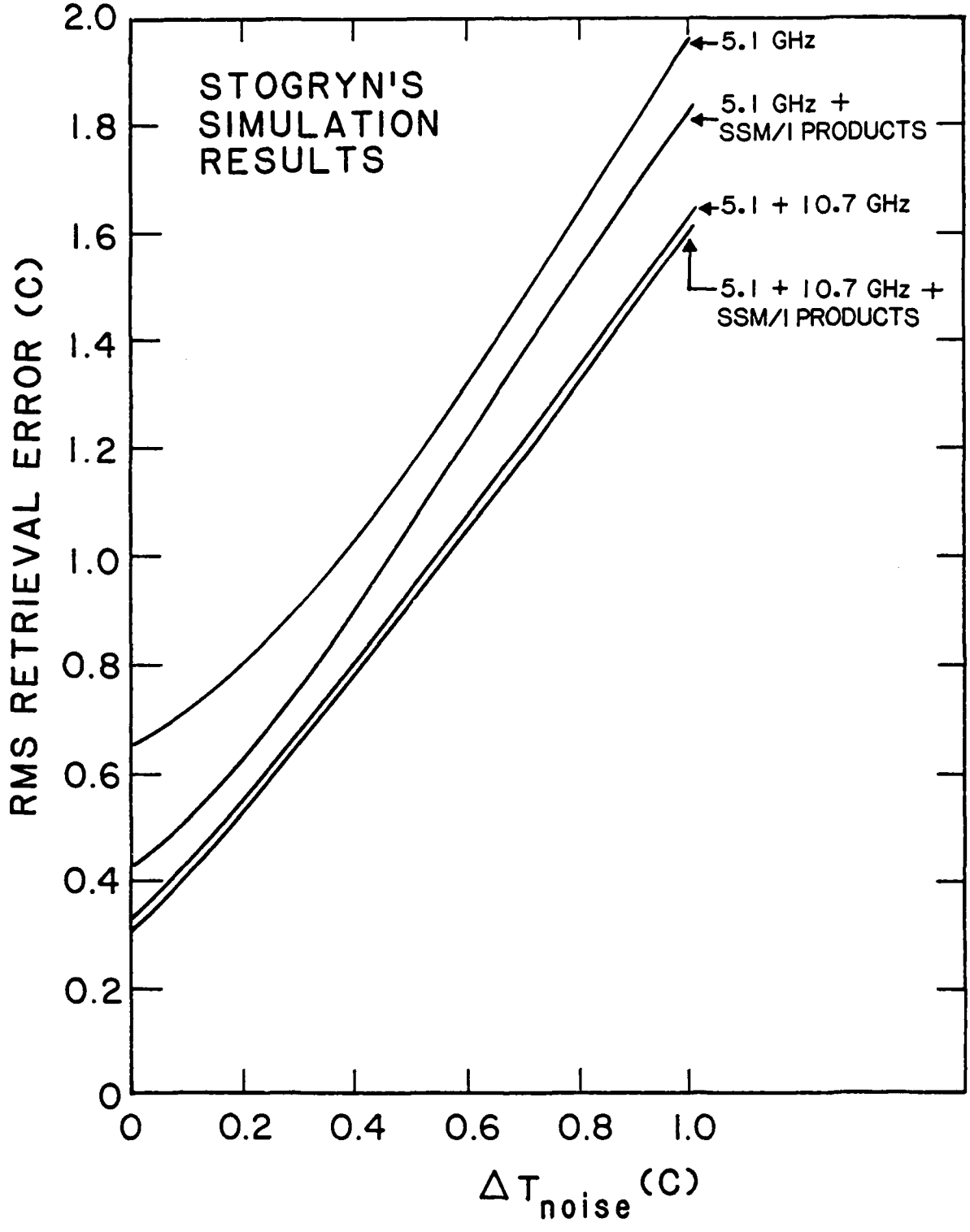

Figure 11 Stogryn's retrieval results for 5.1 GHz and 5.1, 10.7 GHz combination

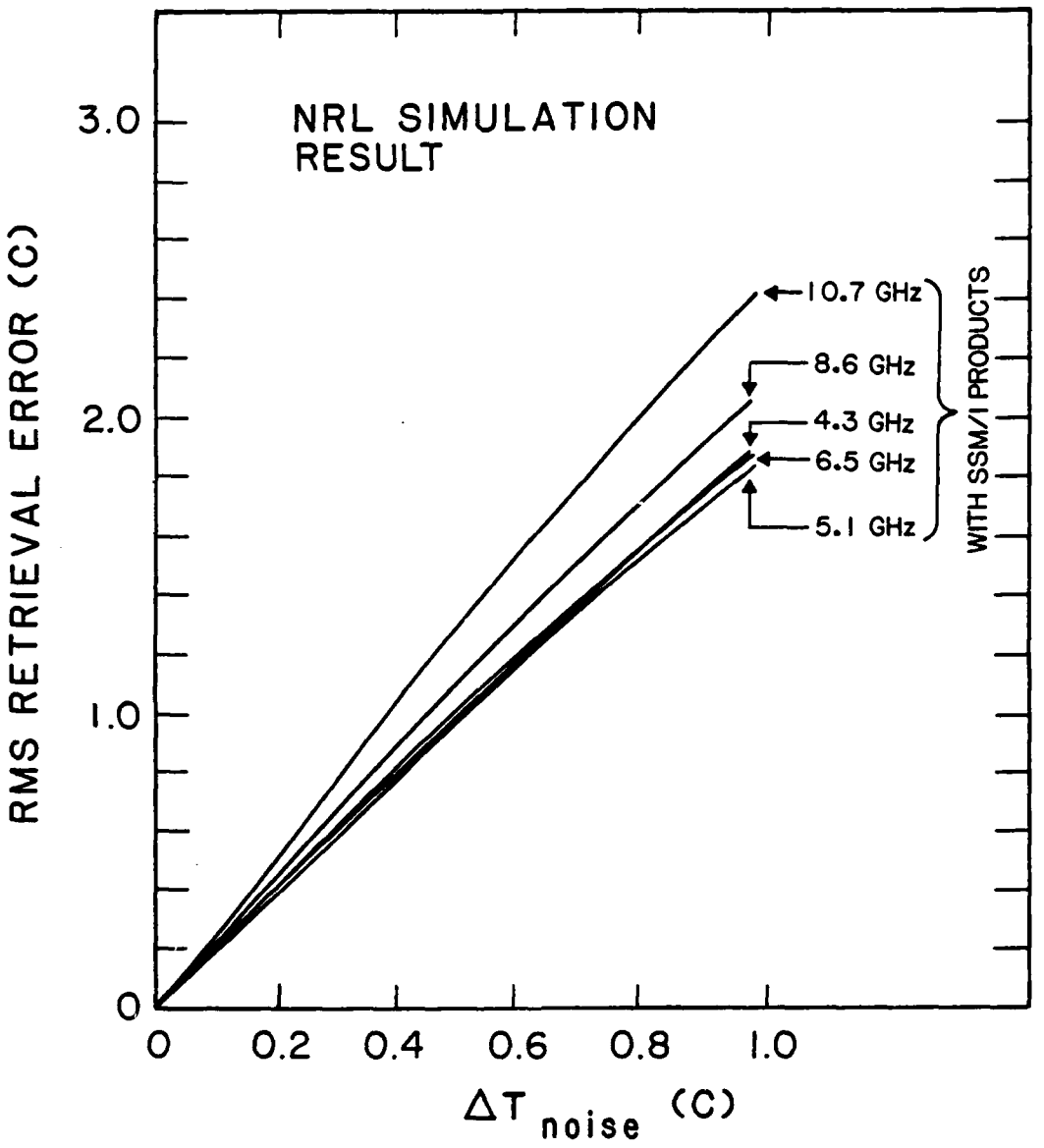

Figure 12 NRL retrieval results for single frequencies

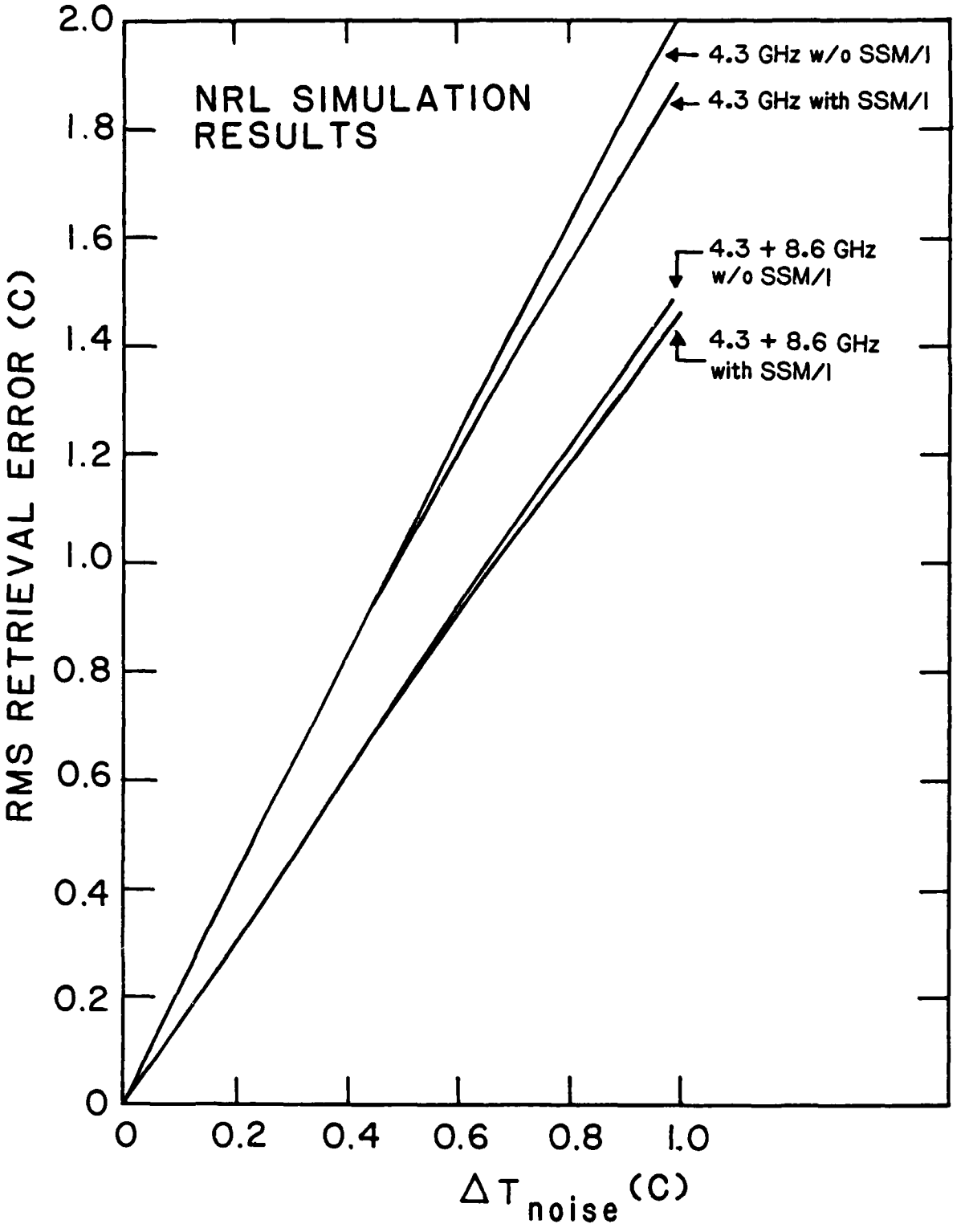

Figure 13 NRL retrieval results for 4.3 GHz and 4.3, 8.6 GHz combination

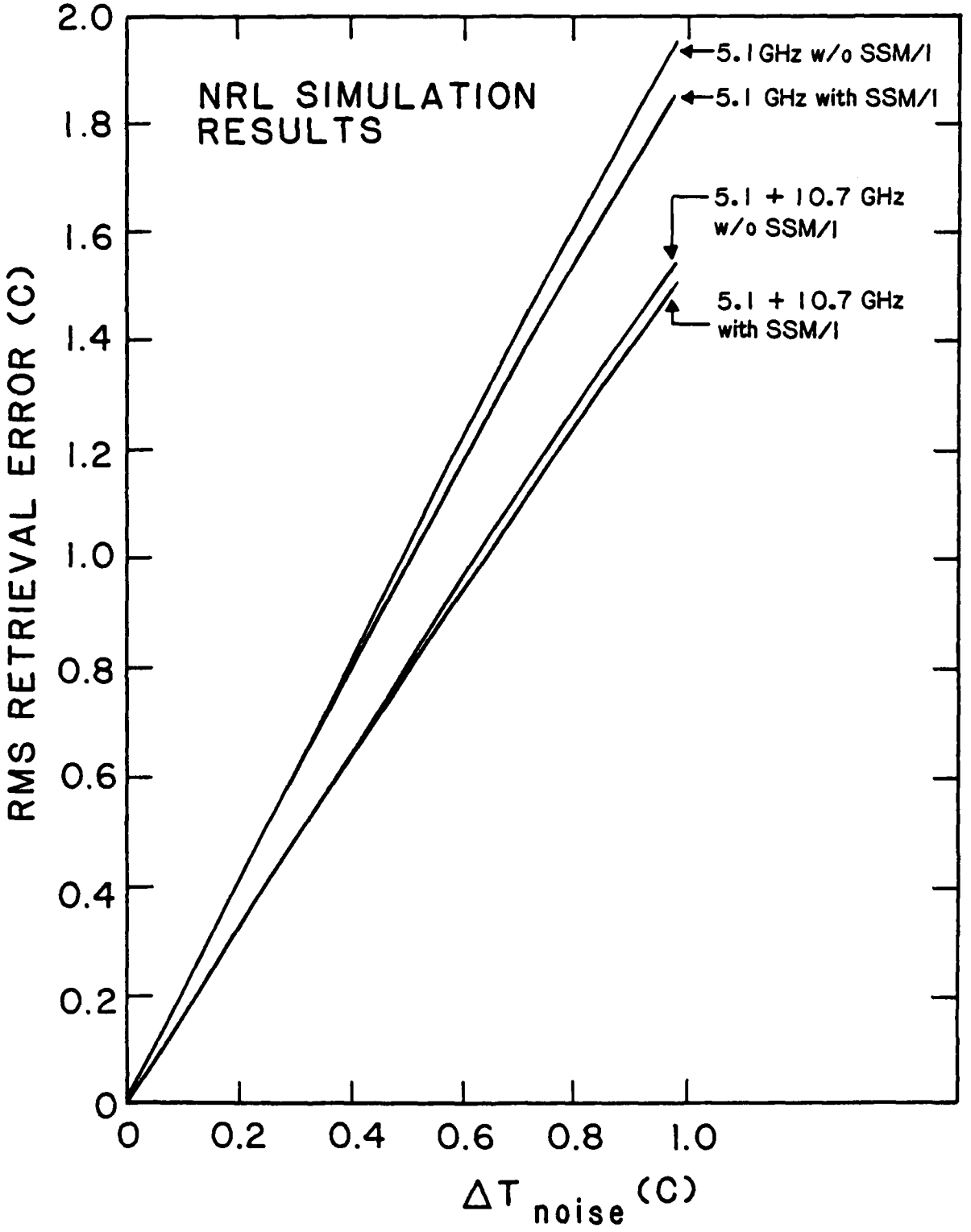

Figure 14 NRL retrieval results for 5.1 GHz and 5.1, 10.7 GHz combination

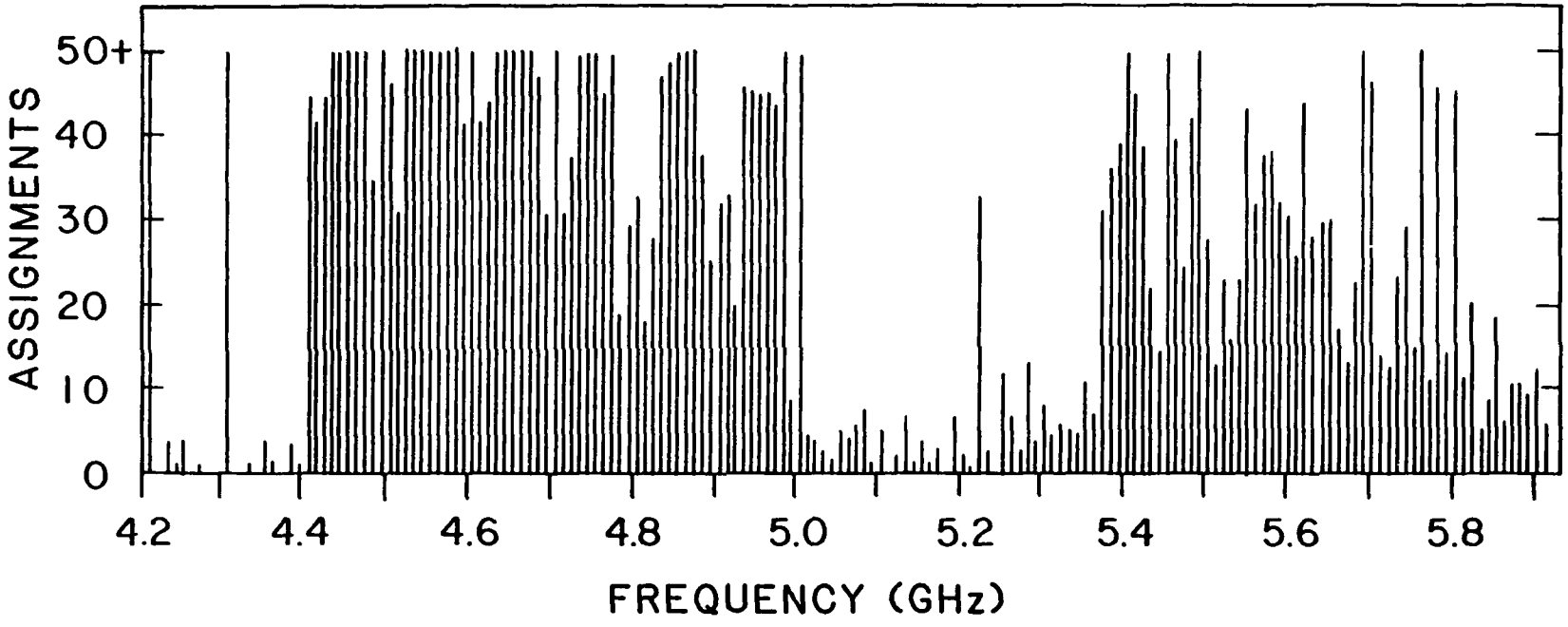

Figure 15 DOD Emitter Survey

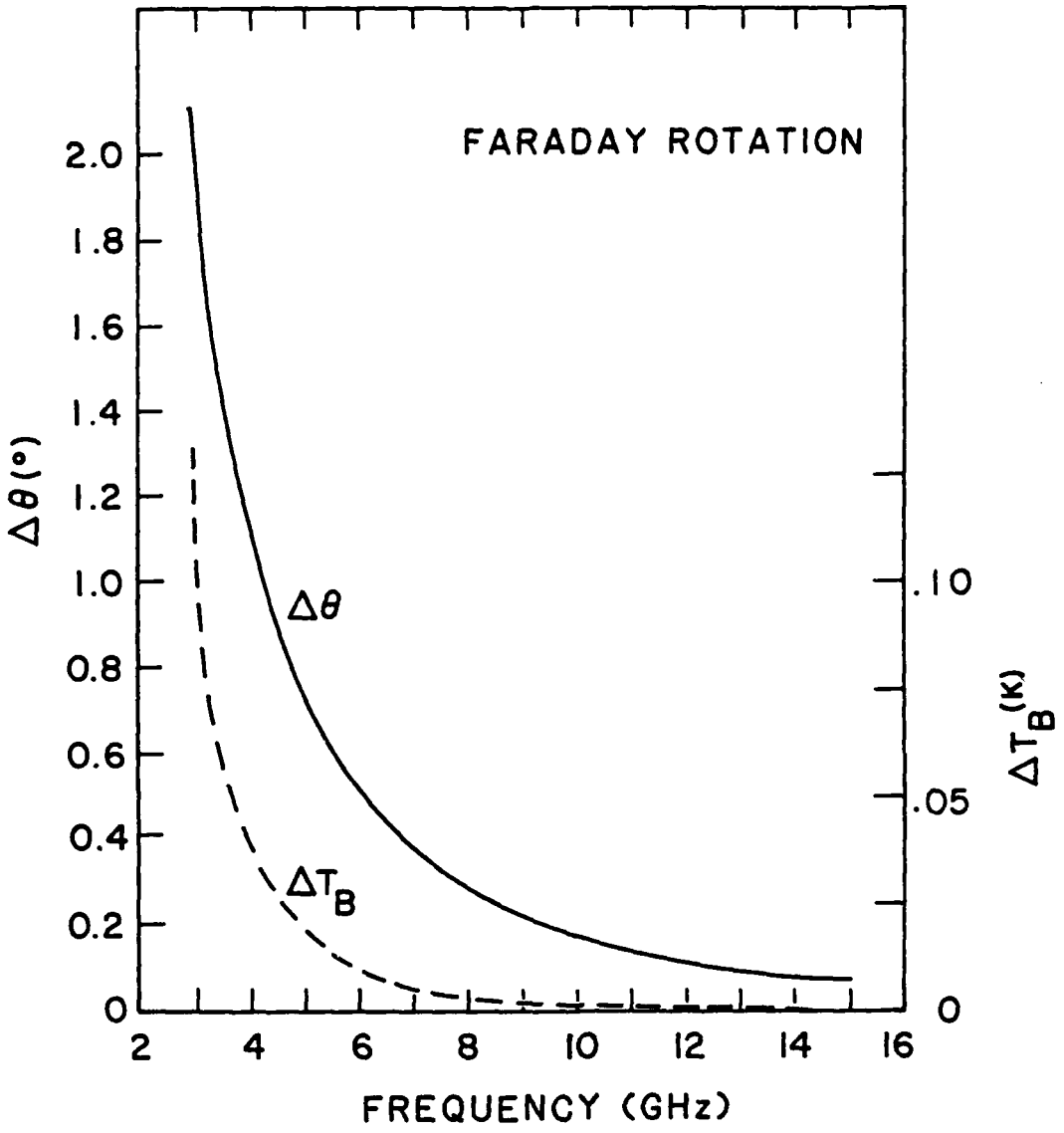

Figure 16 Faraday rotation and resultant error in brightness temperature

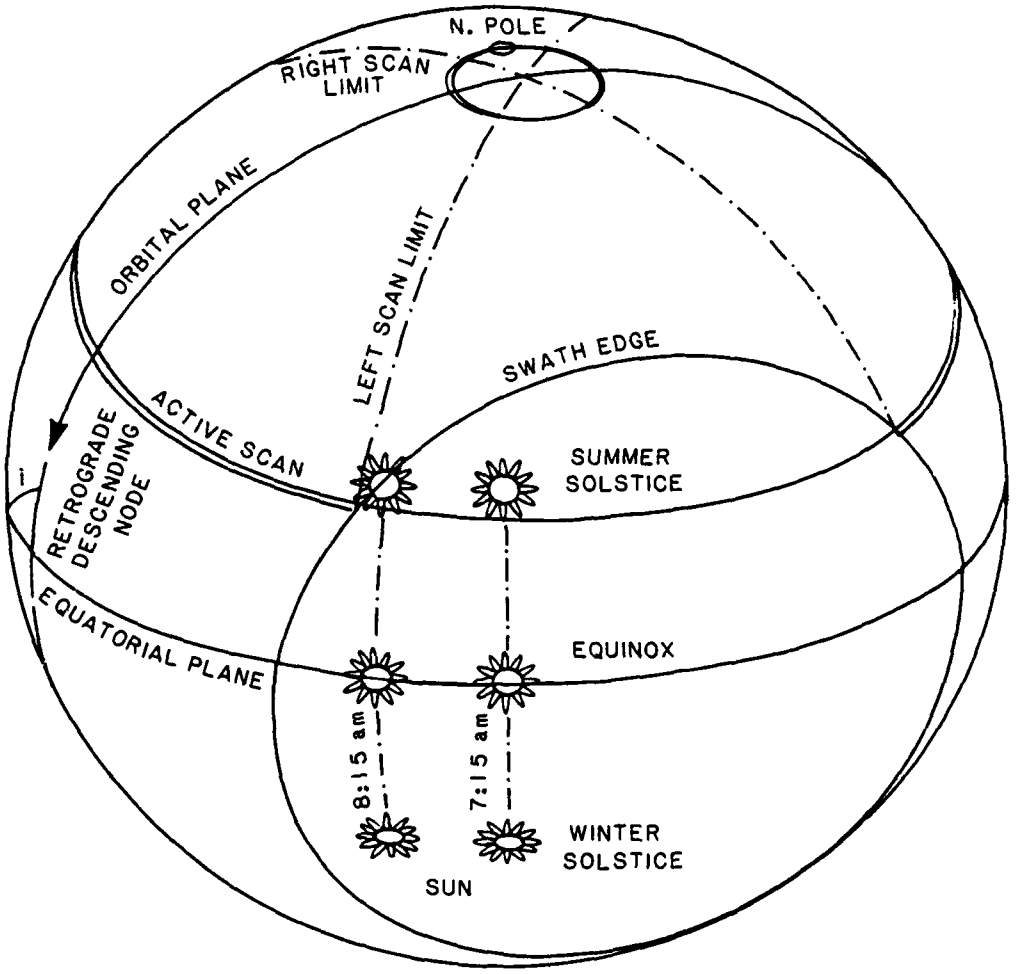

Figure 17 N-ROSS orbit and seasonal sun

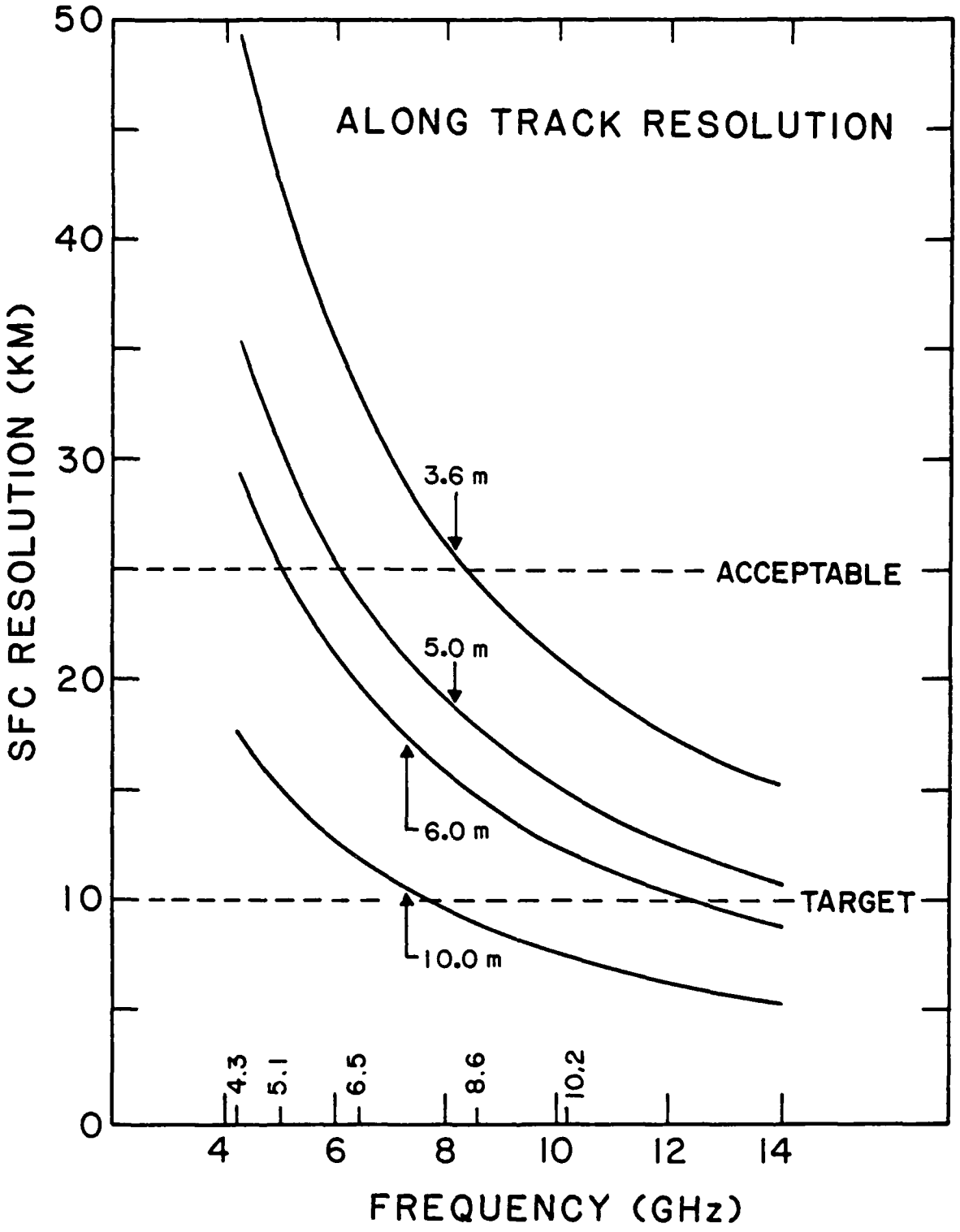

Figure 18 Along track resolution of the LFMR vs antenna sizes

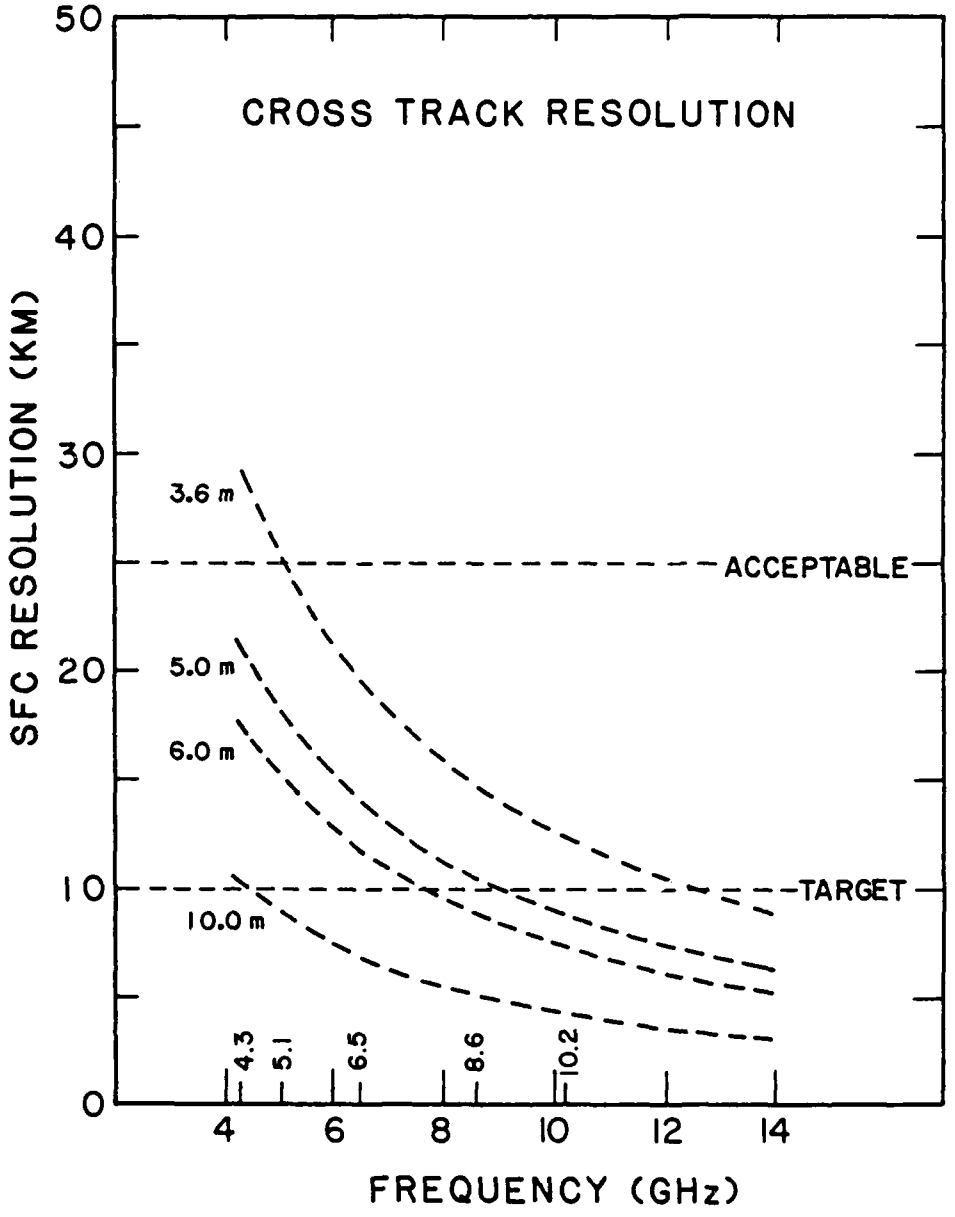

Figure 19 Cross track resolution of the LFMR vs antenna sizes

SCAN A	
SCENE STATIONS/SCAN	128
PIXELS/SCAN	576
SCAN B	
SCENE STATIONS/SCAN	128
PIXELS/SCAN	256
SCENE STATION/ORBIT	404,224
PIXELS/ORBIT	1,313,728

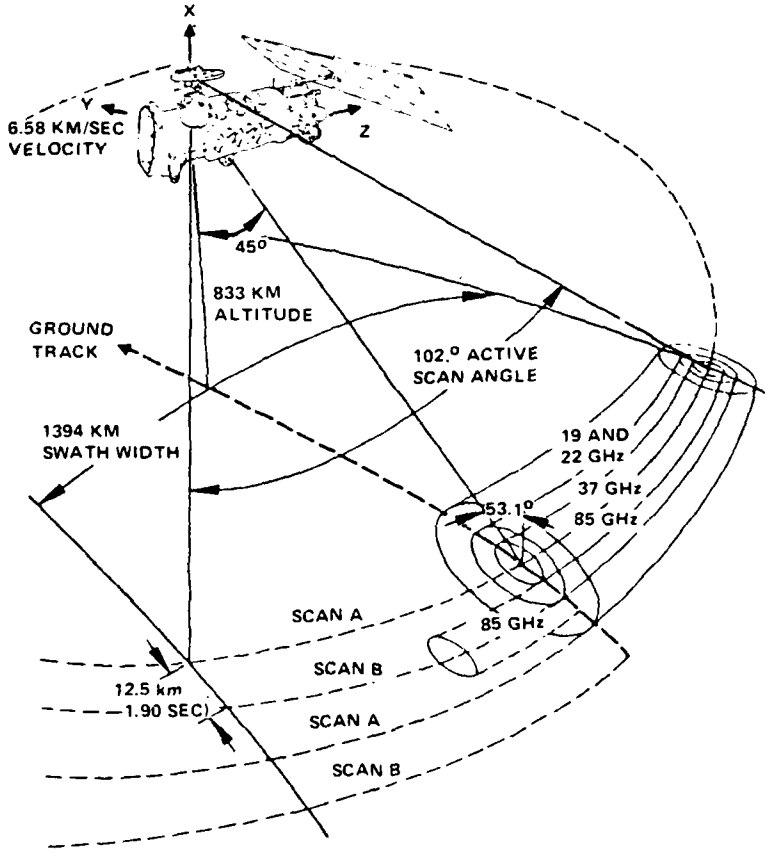

Figure 20 SSM/I scan geometry

3.6 M ANTENNA

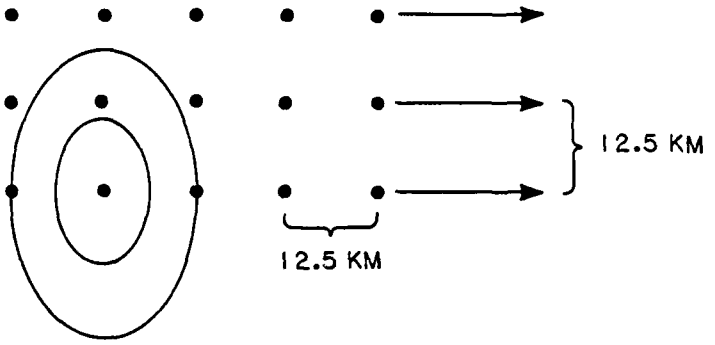

SCAN PERIOD	1.9 SEC
ACTIVE SCAN PERIOD	0.54 SEC
ACTIVE SCAN ANGLE	102.4°

	5.2 GHz	10.4 GHz
BEAM SPOT	25 x 42 Km	13 x 21 Km
NUMBER SAMPLES/SCAN	128	128
LOW PASS FILTER	118 Hz	118 Hz

$$\Delta T \qquad \frac{(250 + 130)K}{\sqrt{(300\times10^6)/(2\times118)}} = 0.34K \qquad \frac{(250 + 150)K}{\sqrt{(500\times10^6)/(2\times118)}} = 0.27K$$

$$\text{DATA RATE} \qquad \frac{2 \times 128 \times 12}{1.9} = 1.6 \text{ KB/S} \qquad \frac{2 \times 128 \times 12}{1.9} = 1.6 \text{ KB/S}$$

TOTAL DATA RATE = 1.6 + 1.6 + 0.5 = 3.7 KB/S

Figure 21 Summary of the LFMR baseline with a 3.6 m antenna

3.6 M ANTENNA

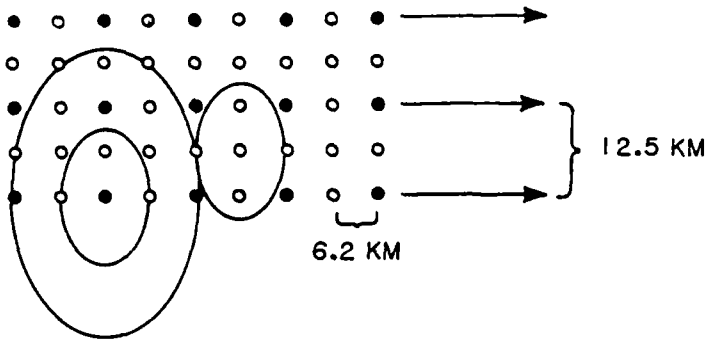

SCAN PERIOD	1.9 SEC
ACTIVE SCAN PERIOD	0.54 SEC
ACTIVE SCAN ANGLE	102.4°

	5.2 GHz	10.4 GHz
BEAM SPOT	25 x 42 KM	13 x 21 KM
NUMBER SAMPLES/SCAN	128	256
LOW PASS FILTER	118 Hz	236 Hz

$$\Delta T \qquad \frac{(250+130)K}{\sqrt{(300\times10^6)/(2\times118)}} = 0.34K \qquad \frac{(250+150)K}{\sqrt{(500\times10^6)/(2\times236)}} = 0.39K$$

$$\text{DATA RATE} \qquad \frac{2\times128\times12}{1.9} = 1.6\ \text{KB/S} \qquad \frac{4\times256\times12}{1.9} = 6.5\ \text{KB/S}$$

TOTAL DATA RATE = 1.6 + 6.5 + 0.5 = 8.6 KB/S

Figure 22 Summary of the LFMR baseline with a 3.6 m antenna using Nyquist sampling

5.9 M ANTENNA

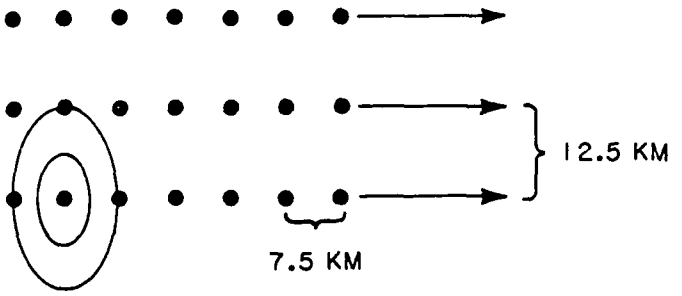

SCAN PERIOD	1.9 SEC
ACTIVE SCAN PERIOD	0.54 SEC
ACTIVE SCAN ANGLE	102.4°

	5.2 GHz	10.4 GHz
BEAM SPOT	15 x 25 KM	8 x 13 KM
NUMBER SAMPLES/SCAN	213	213
LOW PASS FILTER	197 Hz	197 Hz

$$\Delta T \qquad \frac{(250 + 130)K}{\sqrt{(300\times10^6)/(2\times197)}} = 0.44K \qquad \frac{(250 + 150)K}{\sqrt{(500\times10^6)/(2\times197)}} = 0.36K$$

$$\text{DATA RATE} \qquad \frac{2 \times 213 \times 12}{1.9} = 2.7 \text{ KB/S} \qquad \frac{2 \times 213 \times 12}{1.9} = 2.7 \text{ KB/S}$$

TOTAL DATA RATE = 2.7 + 2.7 + 0.5 = 5.9 KB/S

Figure 23 Summary of the LFMR baseline with a 5.9 m antenna

5.9 M ANTENNA

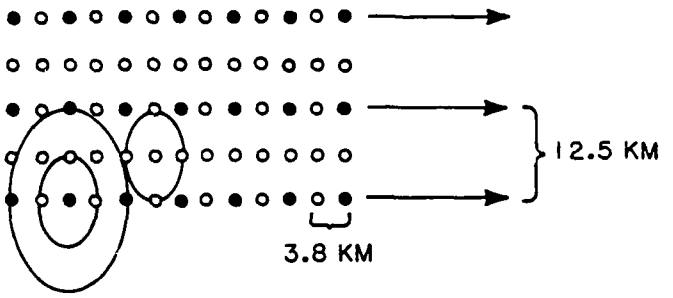

SCAN PERIOD	1.9 SEC
ACTIVE SCAN PERIOD	0.54 SEC
ACTIVE SCAN ANGLE	102.4^{O}

	5.2 GHz	10.4 GHz
BEAMSPOT	15 x 25 KM	8 x 13 KM
NUMBER SAMPLES/SCAN	213	426
LOW PASS FILTER	197 Hz	394 Hz

$$\Delta T \qquad \frac{(250 + 130)K}{\sqrt{(300\times10^{6})/(2\times197)}} = 0.44K \qquad \frac{(250 + 150)K}{\sqrt{(500\times10^{6})/(2\times394)}} = 0.50K$$

$$\text{DATA RATE} \qquad \frac{2 \times 213 \times 12}{1.9} = 2.7 \text{ KB/S} \qquad \frac{4 \times 426 \times 12}{1.9} = 10.8 \text{ KB/S}$$

TOTAL DATA RATE = 2.7 + 10.8 + 0.5 = 14.0 KB/S

Figure 24 Summary of the LFMR baseline with a 5.9 m antenna using Nyquist sampling

References

1. Hofer, R., E.G. Njoku and I.W. Waters, "Microwave Radiometric Measurements of Sea Surface Temperature from the SEASAT Satellite First Results," Science, Vol. 212, June 1981.

2. Hollinger, J.P., R.M. Lerner and M.M. Wisler, "An Investigation of the Remote Determination of Sea Surface Temperature Using Microwave Radiometry," NRL Memorandum Report 3159, Naval Research Laboratory, November 1975.

3. Wisler, M.M., and J.P. Hollinger, "Estimation of Marine Environmental Parameters Using Microwave Radiometric Remote Sensing Systems," NRL Memorandum Report 3661, Naval Research Laboratory, November 1977.

4. Hollinger, J.P., R.M. Lerner, B.E. Troy and M.M. Wisler, "Joint Services 5D-2 Microwave Scanner Definition Study," NRL Memorandum Report 3807, Naval Research Laboratory, August 1978.

5. Bernstein, R.L., "Sea Surface Temperature Mapping with the SEASAT Microwave Radiometer," Journal of Geophysical Research, Vol. 87, No. C10, pp. 7865-7872, September 1982.

6. Wentz, F.J., "Comparison of Sea Surface Temperature Retrievals Using 6.6 and 10.7 GHz," RSS Tech. Report: 092183, Remote Sensing Systems, September 1983.

7. Reynolds, R.W., "A Monthly Averaged Climatology of Sea Surface Temperature," NOAA Technical Report NW S31, June 1982.

8. Reynolds, R.W., "A Comparison of Sea Surface Temperature Climatologies," Journal of Climate and Applied Meteorology, Vol. 22, No. 3, March 1983.

9. Harrington, R.F., "The Development of a Stepped Frequency Microwave Radiometer and its Application to Remote Sensing of the Earth," NASA Technical Memorandum 81847, Langley Research Center, Hampton, VA 23665, June 1980.

10. Stogryn, A., "The Apparent Temperature of the Sea at Microwave Frequencies," IEEE AP-15, No. 2, March 1967.

11. Stogryn, A., "Equations for Calculating the Dielectric Constant of Saline Water at GHz Frequencies," IEEE MTT-19, 1971.

12. Stogryn, A., "A Study of Radiometric Emission from a Rough Sea Surface," NASA Report CR 2088, Langley Research Center, 1972.

13. Stogryn, A., "The Emissivity of Sea Foam at Microwave Frequencies," Journal of Geophysical Research, Vol. 77, No. 9, pp. 16[illegible]566, 1972.

14. Poe, G., "Retrieval Accuracy of Sea Surface Temperature (SST) from Satellite Microwave Radiometer Data," Hughes Aircraft Company 816318-61A, December 1981.

15. Crandall, D., "Survey of Potential Radio Frequency Interference Sources," NRL Memorandum Report No. 4200, Naval Research Laboratory, May 1980.

16. Walton, W. Travis, Personal Communications, 1983.

17. Lawrence, R. S., C. G. Little, and H. J. A. Chivers, "A Survey of Ionospheric Effect Upon Earth-Space Radio Propagation," Proc. IEEE, Vol. 52, pp 4-27, 1964.

18. Allen, C. W., "Astrophysical Quantities," 2nd Edition, The Athlone Press, University of London, 1963.

19. Swift, C. T., H. C. Blume, R. F. Harrington, and C. Jackson, "Sun Glitter and its Effect on Passive Microwave Remote Sensing of the Ocean," Submitted to the NOSS Project, undated.

20. Wentz, F. J., "The Effect of Sea-Surface Sun Glitter on Microwave Radiometer Measurements," Remote Sensing Systems Report No. 110481, November 1981.

21. Hollinger, J. P. and R. C. Lo, "SSM/I Project Summary Report," NRL Memorandum Report 5055, Naval Research Laboratory, April, 1983.

APPENDIX A

COMPARISON OF SEA SURFACE TEMPERATURE RETRIEVALS USING 6.6 AND 10.7 GHz SMMR DATA

Prepared by:

Frank J. Wentz

Remote Sensing Systems
2015 Bridgeway Ste. 302
Sausaltio, CA 94965

1A. INTRODUCTION

The SST measurement capabilities for two microwave radiometer systems are investigated using SEASAT SMMR data. The channels for the two systems are as follows:

System 1 - 6.6 GHz both horizontal and vertical polarization
18.0 GHz vertical polarization
21.0 GHz vertical polarization

System 2 - 10.7 GHz both horizontal and vertical polarization
18.0 GHz vertical polarization
21.0 GHz vertical polarization

The analysis is based on actual SEASAT SMMR T_B's rather than theory. A simple deterministic retrieval algorithm is used to compute SST, given the four SMMR T_B's corresponding to either System 1 or System 2. The SST's inferred from System 1 and from System 2 are then compared with each other and with climatology to determine the relative accuracy of the two systems. In addition, correlation statistics are computed for the 6.6 GHz SST (System 1), the 10.7 GHz SST (System 2), the climatology SST, the 6.6 GHz v-pol T_B, and the 10.7 GHz v-pol T_B.

2A. SEASAT SMMR T_B DATA SET

The SMMR brightness temperatures are averaged onto a 150 km grid aligned with the spacecraft subtrack. Associated with each 150 km cell are 10 T_B's corresponding to the five SMMR frequencies and two polarizations. (In this study only 6 of the 10 T_B's are required.) For each cell, we computed two SST's corresponding to System 1 and System 2, respectively.

For this study, only the highest quality SEASAT SMMR brightness temperatures are used. An objective quality filtering technique is used to obtain this T_B subset. The filtering criteria are as follows:

1. There are four 150 km SMMR T_B cells across the swath. Only the two middle cells are used because the two edge cells suffer from severe polarization coupling due to the SMMR antenna scan design.

2. The T_B cell must be at least 800 km away from land. This eliminates the possibility of sidelobe contamination.

3. Only the nighttime portion of an orbit is used. Faraday rotation, sea-surface sun glitter, sun entering the cold-horn, and thermal gradients aboard the spacecraft all combine to degrade the daytime data.

4. Only measurements coming from the second half of the SEASAT 3-month period are used. During the first half, the 18 GHz channel showed a significant time-dependent drift.

After this filtering, there remains 31781 cells. It is believed that the quality of this T_B subset is indicative of that which will be obtained by future microwave radiometers such as SSM/I and the large aperture N-ROSS radiometer. As such, the data set can be used as a benchmark to evaluate the performance of these instruments.

3A. GEOPHYSICAL RETRIEVAL ALGORITHM

In order to compute SST from the four T_B's reliance is placed upon a simple deterministic inversion algorithm. The inversion problem consists of four equations in four unknowns.

$$TB_i = F_i(SST,W,V,L)$$

where i denotes the channel from 1 to 4. The unknowns SST, W, V, and L denote sea-surface temperature, wind speed, columnar water vapor, and columnar atmospheric liquid water. The T_B function F_i is given by Wentz (1983) and is quasi-linear in SST, W, V, and L. Because of this quasilinearity, the system of equations is easily solved using Newton's method extended to four dimensions.

4A. CLIMATOLOGY SEA SURFACE TEMPERATURE

The SST's computed from the SMMR T_B's are compared to a monthly one degree global SST climatology compiled by Reynolds (1982). This climatology is based on surface marine reports consisting of bucket and engine-intake temperatures. For each month, the SST is given on a 1^o grid extending in latitude from 80 N to 80 S. A bilinear interpolation is used to compute the climatology SST at the center of a 150 km SMMR cell.

5A. INTERCOMPARISON STATISTICS AND ENVIRONMENTAL CASES

In this investigation, six different types of comparisons are made. These are:

1. The 6.6 GHz SST is compared to the climatology SST

2. The 10.7 GHz SST is compared to the climatology SST

3. The 10.7 GHz SST is compared to the 6.6 GHz SST

4. The 6.6 GHz, v-pol T_B is compared to the climatology SST

5. The 10.7 GHz, v-pol is compared to the climatology SST

6. The 10.7 GHz, v-pol is compared to the 6.6 GHz, v-pol T_B

For each type of comparison, ten statistical quantities are computed. To define these quantities, let X and Y denote the two quantities being compared. For comparison 1, X is the 6.6 GHz SST for a given 150 km SMMR cell and Y is the corresponding climatology SST. Futhermore, let N denote the number of SMMR cells being compared, and let <...> denote a simple average over the N cells. The ten statistics are the following:

$\langle X \rangle$ = mean value of X

$\langle Y \rangle$ = mean value of Y

SD(X) = standard deviation of X

$= \text{SQRT}\ (\langle X^2 \rangle - \langle X \rangle^2)$

SD(Y) = standard deviation of Y

$= \text{SQRT}(\langle Y^2 \rangle - \langle Y \rangle^2)$

$\langle Y-X \rangle$ = mean value of Y minus X

SD(Y-X) = standard deviation of Y minus X

$= \text{SQRT}(\langle (Y - X)^2 \rangle - \langle (Y - X) \rangle^2)$

A1 = slope of least-squares linear regression

$= (\langle XY \rangle - \langle X \rangle \langle Y \rangle)/(\langle X^2 \rangle - \langle X \rangle^2)$

A0 = Y intercept of least-squares linear regression

$= \langle Y \rangle - A1 \langle X \rangle$

R = correlation coefficient between X and Y

$= \text{SQRT}((\langle XY \rangle - \langle X \rangle \langle Y \rangle)^2/(\langle X^2 \rangle - \langle X \rangle^2)(\langle Y^2 \rangle - \langle Y \rangle^2))$

Q = standard deviation of Y about the linear regression

$= \text{SQRT}((1 - R^2)(\langle Y^2 \rangle - \langle Y \rangle^2))$

To determine the effect of sea-surface temperature, wind speed, and atmospheric conditions on the SST retrievals, the data are stratified into the following ten environmental cases:

1. Cold water - SST is less than 15°

2. Tepid Water - SST is between 15° and 25°

3. Warm Water - SST is greater than or equal to 25°

4. Clear - columnar atmospheric liquid water is less than 10 mg/cm^2

5. Cloudy - columnar atmospheric liquid water is between 10 and 25 mg/cm^2

6. Rain - columnar atmospheric liquid water is greater than or equal to 25 mg/cm^2

7. Light wind - wind is less than 7 m/s

8. Medium wind - wind is between 7 and 14 m/s

9. High wind - wind is greater than or equal to 14 m/s

10. All 31781 cells, regardless of environmental conditions

The climatology SST is used to specify the sea-surface temperature stratification. The wind speed and columnar atmospheric liquid water that are computed from the T_B's for system 2 are used to specify the wind and the atmospheric stratification.

6A. RESULTS

Tables 1 through 6 show the statistics from the six types of comparisons listed in Section 5, respectively. In each table, the statistics are given for the ten environmental cases. In analyzing the tables, focus on the column labeled SD(Y-X), which is the standard deviation of the difference between the two parameters being compared. Table 1 shows that the overall agreement between the 6.6 GHz SST and climatology is 1.58 C. The agreement is better for warm water than cold water (1.24 C compared to 1.85 C). There is a slight degradation in the comparisons going from clear skies to rain. Furthermore, the high wind case shows poorer agreement than the light wind case. It should be noted that the average climatology SST for high winds in 10.31 C. Thus the poor agreement for high winds may be due to the cold water rather than the wind. The comparisons of the 10.7 GHz SST with climatology given in Table 2 show a stronger dependence on SST. The agreement degrades from 1.17 C to 2.37 C when going from warm to cold water. In Table 3 the 10.7 GHz SST is compared to the 6.6 GHz SST. The agreement between the two SST estimates is better than that obtained for the climatology comparisons, probably because of errors in the climatology. For warm water the variation between the two estimates is only 1.09 C, and in cold water this figure increases to 1.78 C.

The bias term <X-Y> in Tables 1 through 3 also varies in going from warm to cold water. This variation in the mean SST difference is probably due to small systematic errors in the T_B model function F_i used in the retrieval algorithm and/or regional differences between the actual SST and climatology.

Tables 4 through 6 give the statistics for the brightness temperature comparisons. For these tables, the important statistic is the correlation R. The overall correlation between the 6.6 GHz v-pol T_B and the climatology SST is 0.8980, which is higher than the 0.7853 correlation obtained in Table 5 for the 10.7 GHz T_B. The lower correlation for 10.7 GHz is due to two

factors. First, as compared to 6.6 GHz, the 10.7 GHz v-pol T_B is about three times more sensitive to variations in the atmosphere (i.e., water vapor, clouds, and rain). Second, as shown by Tables 1 and 2, the 10.7 GHz v-pol T_B is overall less sensitive to SST because of the cold water cases. It should be noted that due to the restricted range of SST for the cold, tepid, and warm water cases, the correlations for these cases are smaller than the correlation for the 'all' case, which has three times the dynamic range in SST. Table 6 compares the 6.6 and 10.7 T_B's. The overall correlation between these two channels is quite high, being 0.9538.

Plots of the six comparisons appear in Figures 1 through 6. In generating these plots, the 31781 cells are stratified into 1^o bins along the X axis. Table 7 gives the mean X value <X> and the number of samples for each bin appearing in Figures 1 through 6. The mean Y value <Y> and standard deviation of Y are also found for each bin. The error bars in the figures are drawn such that their center is at the point <X>,<Y> and their length is twice the standard deviation of Y. Thus the error bars represent the $\pm$ one sigma variation of Y. In Figures 1 through 3, the large error bars for cold water again show that the SST retrieval degrades for temperatures below 15^o C, particular for 10.7 GHz. Figures 4 and 5 clearly show how the T_B versus SST relationship flattens out for cold water, which is the cause for the poor SST retrieval. The interpretation of Figure 6, which plots the 10.7 GHz T_B versus the 6.6 GHz T_B, is less straightforward. The error bars are the smallest for the lower T_B values, which are associated with cold water, light winds, and low water vapor content. It thus appears that the 6.6 to 10.7 GHz T_B variation is less for regions having cold water, light winds, and low vapor.

7A. CONCLUSIONS

The SST performance of the 6.6 GHz and the 10.7 GHz radiometer systems depends on the water temperature. The performance is better for warm water than cold water. The degradation of the 10.7 GHz system in cold water is more serious than for the 6.6 GHz system. The one sigma variations among the 6.6 GHz SST, the 10.7 GHz SST, and climatology for water temperatures less than 15 C and greater then 15 C are summarized as follows:

	< 15 C	> 15 C
6.6 GHz system compared to climatology	1.85 C	1.34 C
10.7 GHz system compared to climatology	2.37 C	1.49 C
10.7 GHz system compared to 6.6 GHz system	1.78 C	1.17 C

Note the above figures do <u>not</u> represent the actual accuracy of the retrieved SST compared to truth because of the existance of real SST anomalies with respect to climatology. However, it is clear from the figures that the performance of the 10.7 GHz system is about the same as the 6.6 GHz system for warm water and is worse than the 6.6 GHz system for cold water.

It is interesting to note that for SST > 15 C, the agreement between the two systems is 1.17 C. If the errors in the retrievals for the two

systems are uncorrelated, random, and of the same magnitude, then the 1.17 C difference can be equally partitioned. That is, it can be assumed that Systems 1 and 2 each have an error of 1.17/ 2 = 0.83 C. If the SST estimates from the two systems were averaged, then the 0.83 C error for a single system would be reduced by 2. Thus by using both 6.6 and 10.7 GHz, the SST retrieval error would be 0.58 C. However, in order to achieve this high degree of accuracy, all systematic errors in the retrieval process must be eliminated.

REFERENCES

1. Reynolds, R. W., "A Monthly Averaged Climatology of Sea Surface Temperature," NOAA Technical Report NWS 31, June, 1982.

2. Wentz, F. J., "A Model Function for Ocean Microwave Brightness Temperatures," Journal of Geophysical Research, 88(C3), pp. 1892-1908, February 1983.

TABLE 1

STATISTICS ON 6.6 GHZ SST VERSUS CLIMATOLOGY SST

	N	<X>	<Y>	SD(X)	SD(Y)	<Y-X>	SD(Y-X)	A0	A1	R	Q
COLD WATER	9022	9.78	10.63	3.10	3.65	0.85	1.85	0.70	1.0152	0.8623	1.85
TEPID WATER	12795	20.69	20.58	2.87	2.70	-0.11	1.40	3.53	0.8239	0.8764	1.30
WARM WATER	9964	27.05	26.62	1.14	1.77	-0.43	1.24	-3.87	1.1269	0.7209	1.23
CLEAR	24898	18.81	18.78	7.11	6.74	-0.03	1.51	1.34	0.9270	0.9777	1.42
CLOUDY	6244	22.33	22.69	6.75	6.07	0.35	1.78	3.27	0.8697	0.9670	1.55
RAIN	639	22.91	23.65	6.93	6.21	0.73	1.77	3.74	0.8686	0.9698	1.51
LIGHT WIND	17066	22.34	22.23	5.79	5.56	-0.12	1.38	1.38	0.9330	0.9711	1.33
MEDIUM WIND	12253	17.62	17.86	7.16	6.61	0.25	1.70	2.04	0.8980	0.9728	1.53
HIGH WIND	2462	10.31	10.67	4.73	4.93	0.36	2.05	0.89	0.9487	0.9105	2.04
ALL	31781	19.59	19.65	7.19	6.81	0.06	1.58	1.55	0.9240	0.9760	1.48

X = Reynold's Climatology SST

Y = SST inferred from 6.6 H, 6.6 V, 18 V, and 21 V SMMR Channels

TABLE 2

STATISTICS ON 10.7 GHZ SST VERSUS CLIMATOLOGY SST

	N	<X>	<Y>	SD(X)	SD(Y)	<Y-X>	SD(Y-X)	A0	A1	R	Q
COLD WATER	9022	9.78	11.08	3.10	4.01	1.30	2.37	0.88	1.0432	0.8065	2.37
TEPID WATER	12795	20.69	20.55	2.87	2.56	-0.14	1.63	5.34	0.7352	0.8263	1.44
WARM WATER	9964	27.05	26.22	1.14	1.76	-0.83	1.17	-5.21	1.1618	0.7507	1.16
CLEAR	24898	18.81	18.85	7.11	6.54	0.04	1.89	2.16	0.8874	0.9651	1.71
CLOUDY	6244	22.33	22.40	6.75	5.70	0.07	2.14	4.39	0.8065	0.9546	1.70
RAIN	639	22.91	23.21	6.93	5.98	0.29	2.24	4.41	0.8201	0.9507	1.86
LIGHT WIND	17066	22.34	22.18	5.79	5.13	-0.16	1.68	3.18	0.8503	0.9598	1.44
MEDIUM WIND	12253	17.62	17.98	7.16	6.29	0.36	2.10	3.14	0.8422	0.9595	1.77
HIGH WIND	2462	10.31	10.31	4.73	5.38	-0.00	2.60	0.05	0.9951	0.8752	2.60
ALL	31781	19.59	19.64	7.19	6.55	0.05	1.95	2.45	0.8775	0.9641	1.74

X = Reynold's Climatology SST

Y = SST inferred from 10.7 H, 10.7 V, 18 V, and 21 V SMMR Channels

TABLE 3

STATISTICS ON 10.7 GHZ SST VERSUS 6.6 GHZ SST

	N	<X>	<Y>	SD(X)	SD(Y)	<Y-X>	SD(Y-X)	A0	A1	R	Q
COLD WATER	9022	10.63	11.08	3.65	4.01	0.45	1.78	0.61	0.9848	0.8964	1.78
TEPID WATER	12795	20.58	20.55	2.70	2.56	-0.03	1.21	3.10	0.8481	0.8961	1.13
WARM WATER	9964	26.62	26.22	1.77	1.76	-0.40	1.09	4.91	0.8007	0.8088	1.03
CLEAR	24898	18.78	18.85	6.74	6.54	0.07	1.40	1.03	0.9487	0.9783	1.36
CLOUDY	6244	22.69	22.40	6.07	5.70	-0.28	1.36	1.62	0.9162	0.9753	1.26
RAIN	639	23.65	23.21	6.21	5.98	-0.44	1.45	1.06	0.9367	0.9725	1.39
LIGHT WIND	17066	22.23	22.18	5.56	5.13	-0.05	1.30	2.22	0.8979	0.9737	1.17
MEDIUM WIND	12253	17.86	17.98	6.61	6.29	0.12	1.41	1.38	0.9294	0.9774	1.33
HIGH WIND	2462	10.67	10.31	4.93	5.38	-0.37	1.89	-0.60	1.0217	0.9364	1.89
ALL	31781	19.65	19.64	6.81	6.55	-0.01	1.40	1.15	0.9410	0.9788	1.34

X = SST inferred from 6.6 H, 6.6 V, 18 V, and 21 V SMMR Channels

Y = SST inferred from 10.7 H, 10.7 V, 18 V, and 21 V SMMR Channels

TABLE 4

STATISTICS ON 6.6 GHZ V-POL TB VERSUS CLIMATOLOGY SST

	N	<X>	<Y>	SD(X)	SD(Y)	<Y-X>	SD(Y-X)	A0	A1	R	Q
COLD WATER	9022	9.78	149.73	3.10	2.41	139.95	2.95	146.31	0.3492	0.4489	2.15
TEPID WATER	12795	20.69	153.95	2.87	1.90	133.25	1.96	143.91	0.4853	0.7348	1.29
WARM WATER	9964	27.05	157.54	1.14	1.20	130.49	1.05	140.29	0.6379	0.6012	0.96
CLEAR	24898	18.81	153.28	7.11	3.49	134.46	4.15	144.80	0.4504	0.9175	1.39
CLOUDY	6244	22.33	155.87	6.75	2.84	133.54	4.65	148.03	0.3513	0.8354	1.56
RAIN	639	22.91	157.70	6.93	2.68	134.78	5.06	150.61	0.3090	0.7984	1.62
LIGHT WIND	17066	22.34	154.50	5.79	3.38	132.16	2.67	141.90	0.5641	0.9657	0.88
MEDIUM WIND	12253	17.62	153.25	7.16	3.74	135.63	3.81	144.53	0.4946	0.9468	1.20
HIGH WIND	2462	10.31	152.68	4.73	2.92	142.37	3.19	147.90	0.4633	0.7513	1.93
ALL	31781	19.59	153.88	7.19	3.56	134.29	4.29	145.17	0.4445	0.8980	1.57

X = Reynold's Climatology SST

Y = 6.6 V SMMR TB

TABLE 5

STATISTICS ON 10.7 GHZ V-POL TB VERSUS CLIMATOLOGY SST

	N	<X>	<Y>	SD(X)	SD(Y)	<Y-X>	SD(Y-X)	A0	A1	R	Q
COLD WATER	9022	9.78	156.74	3.10	2.67	146.96	3.59	154.79	0.1996	0.2316	2.60
TEPID WATER	12795	20.69	159.59	2.87	2.06	138.89	2.41	151.18	0.4065	0.5656	1.70
WARM WATER	9964	27.05	163.36	1.14	1.77	136.30	1.44	138.84	0.9061	0.5815	1.44
CLEAR	24898	18.81	159.23	7.11	3.13	140.42	4.82	152.33	0.3668	0.8339	1.73
CLOUDY	6244	22.33	162.26	6.75	2.67	139.93	5.50	156.77	0.2461	0.6230	2.09
RAIN	639	22.91	165.81	6.93	2.51	142.89	5.94	161.26	0.1984	0.5484	2.10
LIGHT WIND	17066	22.34	160.23	5.79	3.34	137.89	3.05	148.43	0.5280	0.9151	1.35
MEDIUM WIND	12253	17.62	159.58	7.16	3.45	141.97	4.55	152.28	0.4143	0.8602	1.76
HIGH WIND	2462	10.31	159.98	4.73	2.93	149.67	3.78	156.13	0.3727	0.6025	2.34
ALL	31781	19.59	159.96	7.19	3.37	140.37	5.00	152.76	0.3674	0.7853	2.08

X = Reynold's Climatology SST

Y = 10.7 V SMMR TB

TABLE 6

STATISTICS ON 10.7 GHZ V-POL TB VERSUS 6.6 GHZ V-POL TB

	N	<X>	<Y>	SD(X)	SD(Y)	<Y-X>	SD(Y-X)	A0	A1	R	Q
COLD WATER	9022	149.73	156.74	2.41	2.67	7.02	1.01	3.17	1.0257	0.9260	1.01
TEPID WATER	12795	153.95	159.59	1.90	2.06	5.64	0.79	4.74	1.0058	0.9245	0.79
WARM WATER	9964	157.54	163.36	1.20	1.77	5.81	0.90	-41.31	1.2991	0.8845	0.83
CLEAR	24898	153.28	159.23	3.49	3.13	5.95	0.93	26.48	0.8661	0.9668	0.80
CLOUDY	6244	155.87	162.26	2.84	2.67	6.39	1.23	30.30	0.8466	0.9013	1.16
RAIN	639	157.70	165.81	2.68	2.51	8.11	1.31	36.85	0.8178	0.8748	1.21
LIGHT WIND	17066	154.50	160.23	3.38	3.34	5.73	0.88	12.86	0.9538	0.9657	0.87
MEDIUM WIND	12253	153.25	159.58	3.74	3.45	6.34	1.06	23.97	0.8849	0.9599	0.97
HIGH WIND	2462	152.68	159.98	2.92	2.93	7.30	1.06	16.85	0.9375	0.9345	1.04
ALL	31781	153.88	159.96	3.56	3.37	6.08	1.07	21.22	0.9016	0.9538	1.01

X = 6.6 V SMMR TB

Y = 10.7 V SMMR TB

TABLE 7. Number of Samples for Error Bars in Plots

Fig. 1,2,4,5			Fig. 3			Fig. 6		
SSTCY		number	SST6		number	TB6V		number
1.66	-	16	1.57	-	47	143.76	-	5
2.62	-	100	2.56	-	108	144.62	-	84
3.52	-	175	3.51	-	183	145.57	-	298
4.53	-	365	4.53	-	272	146.54	-	734
5.55	-	395	5.50	-	423	147.53	-	1103
6.56	-	707	6.54	-	542	148.52	-	1373
7.49	-	1004	7.52	-	655	149.52	-	1761
8.48	-	1120	8.49	-	737	150.51	-	2040
9.47	-	852	9.48	-	822	151.52	-	2359
10.48	-	847	10.48	-	858	152.50	-	2534
11.52	-	827	11.51	-	864	153.50	-	2628
12.49	-	843	12.50	-	884	154.49	-	2699
13.50	-	885	13.52	-	886	155.52	-	3195
14.50	-	886	14.51	-	898	156.52	-	3856
15.51	-	904	15.51	-	916	157.47	-	3594
16.50	-	938	16.50	-	1082	158.45	-	2309
17.50	-	1005	17.49	-	1164	159.39	-	940
18.50	-	1140	18.52	-	1343	160.38	-	193
19.47	-	1018	19.51	-	1494	161.41	-	47
20.51	-	1188	20.50	-	1691	162.40	-	25
21.50	-	1577	21.50	-	1739			
22.49	-	1547	22.50	-	1787			
23.51	-	1582	23.50	-	1816			
24.53	-	1896	24.50	-	1963			
25.48	-	2188	25.51	-	2165			
26.51	-	2330	26.50	-	2237			
27.50	-	3393	27.47	-	1981			
28.41	-	1561	28.45	-	1301			
29.26	-	492	29.42	-	634			
			30.39	-	211			
			31.51	-	35			
			32.35	-	12			

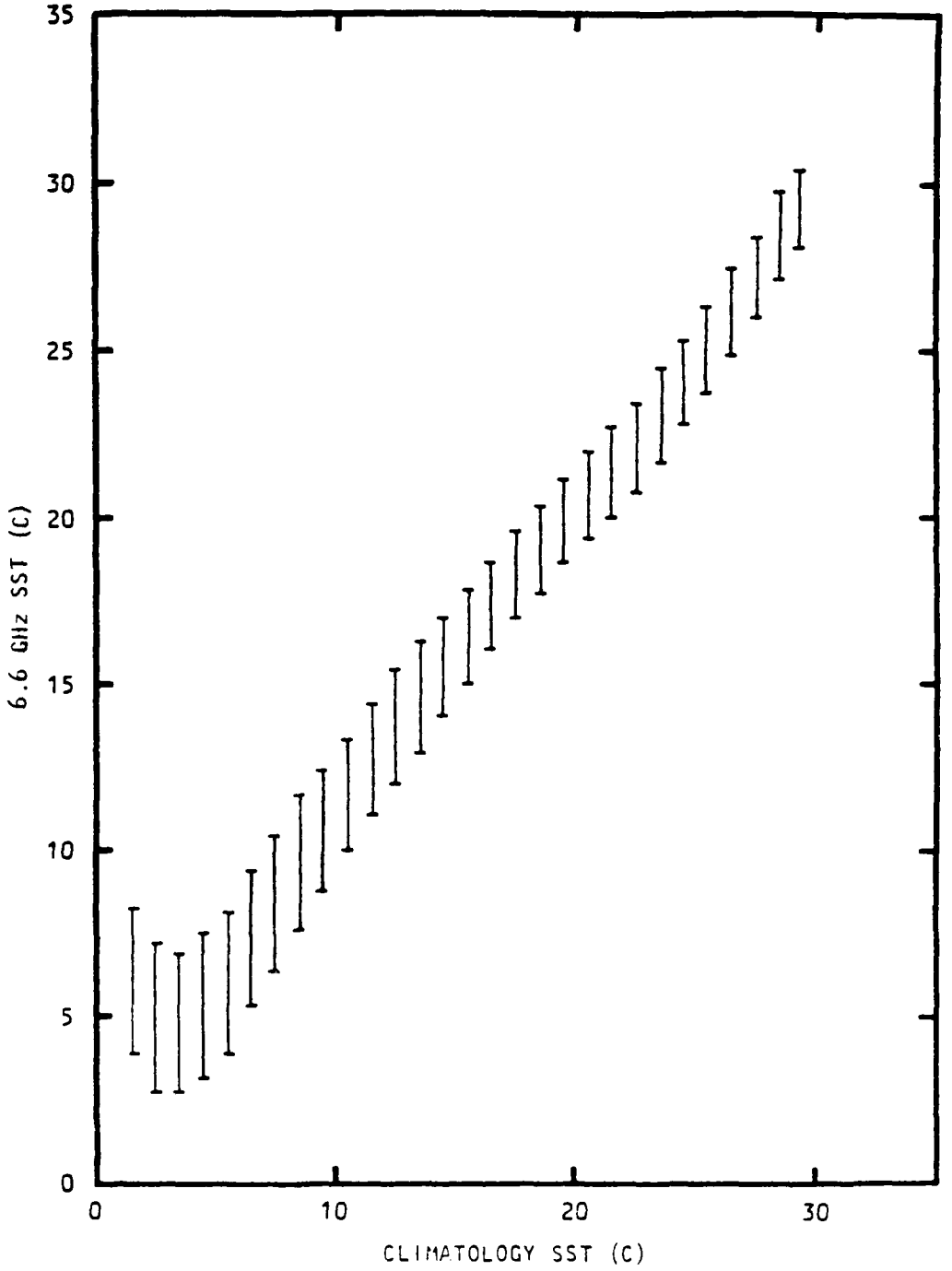

Fig. 1. Comparison of 6.6 GHz SST versus Climatology SST.

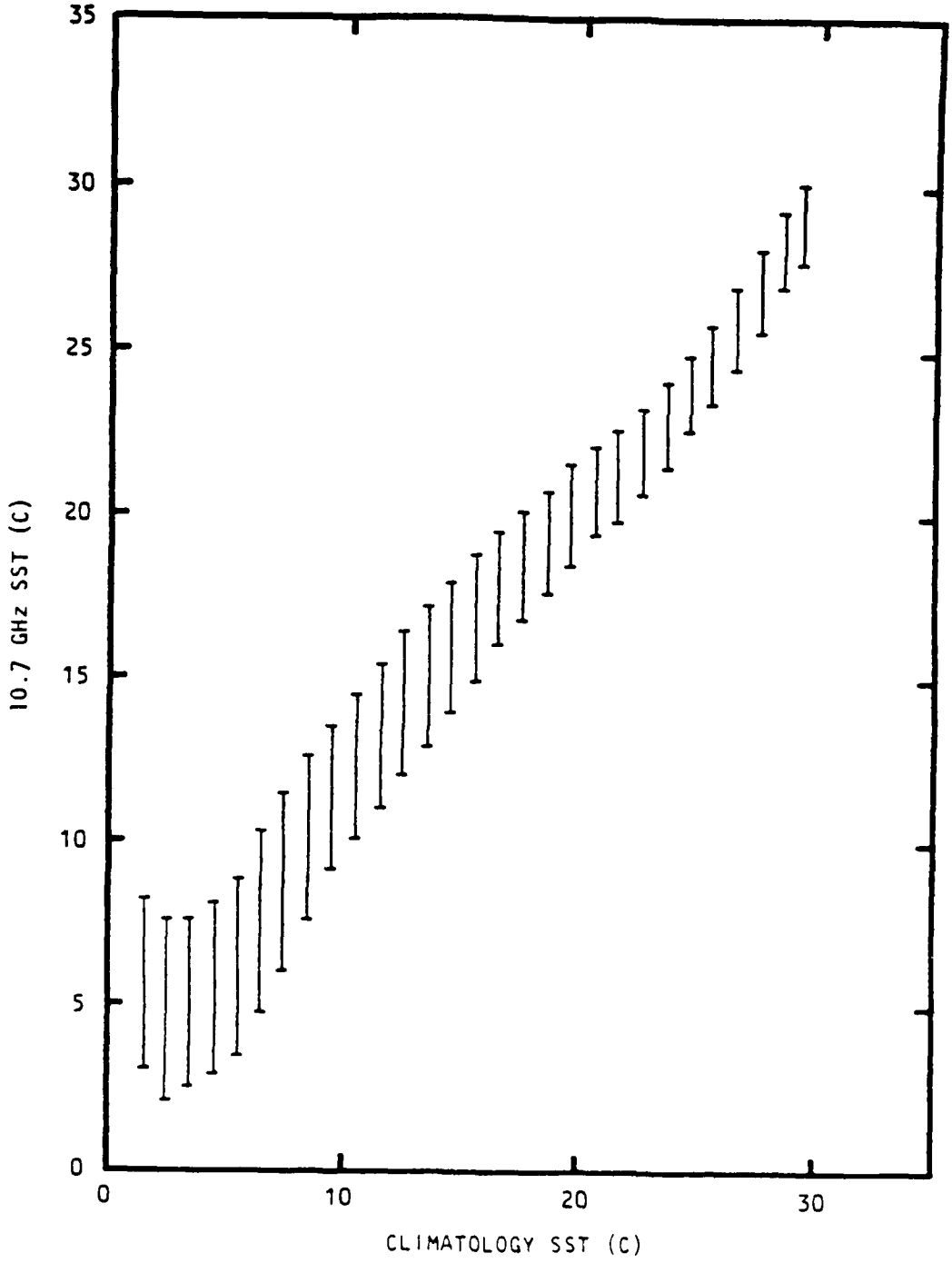

Fig. 2. Comparison of 10.7 GHz SST versus Climatology SST.

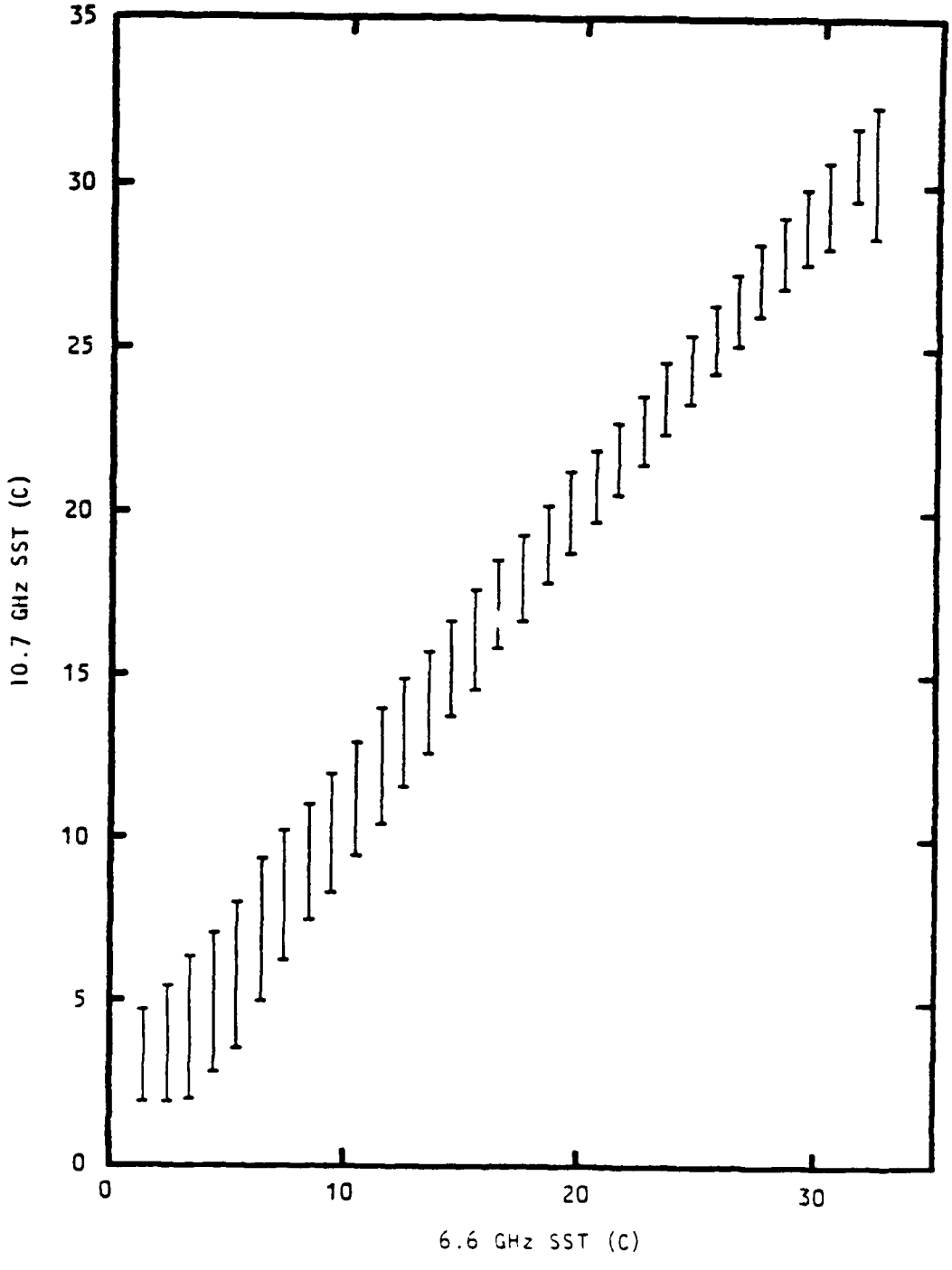

Fig. 3. Comparison of 10.7 GHz SST versus 6.6 GHz SST.

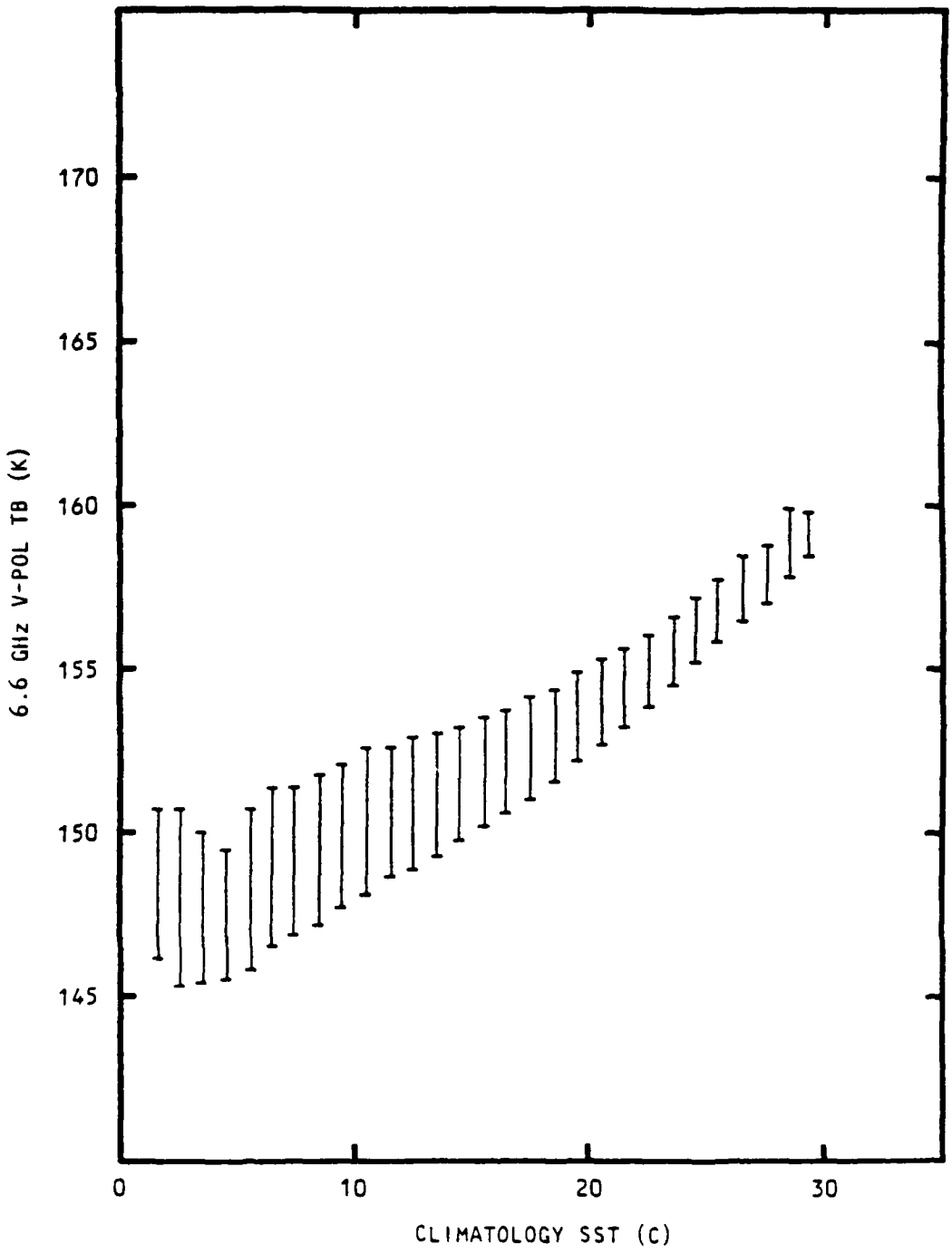

Fig. 4. Comparison of 6.6 GHz v-pol TB versus Climatology SST.

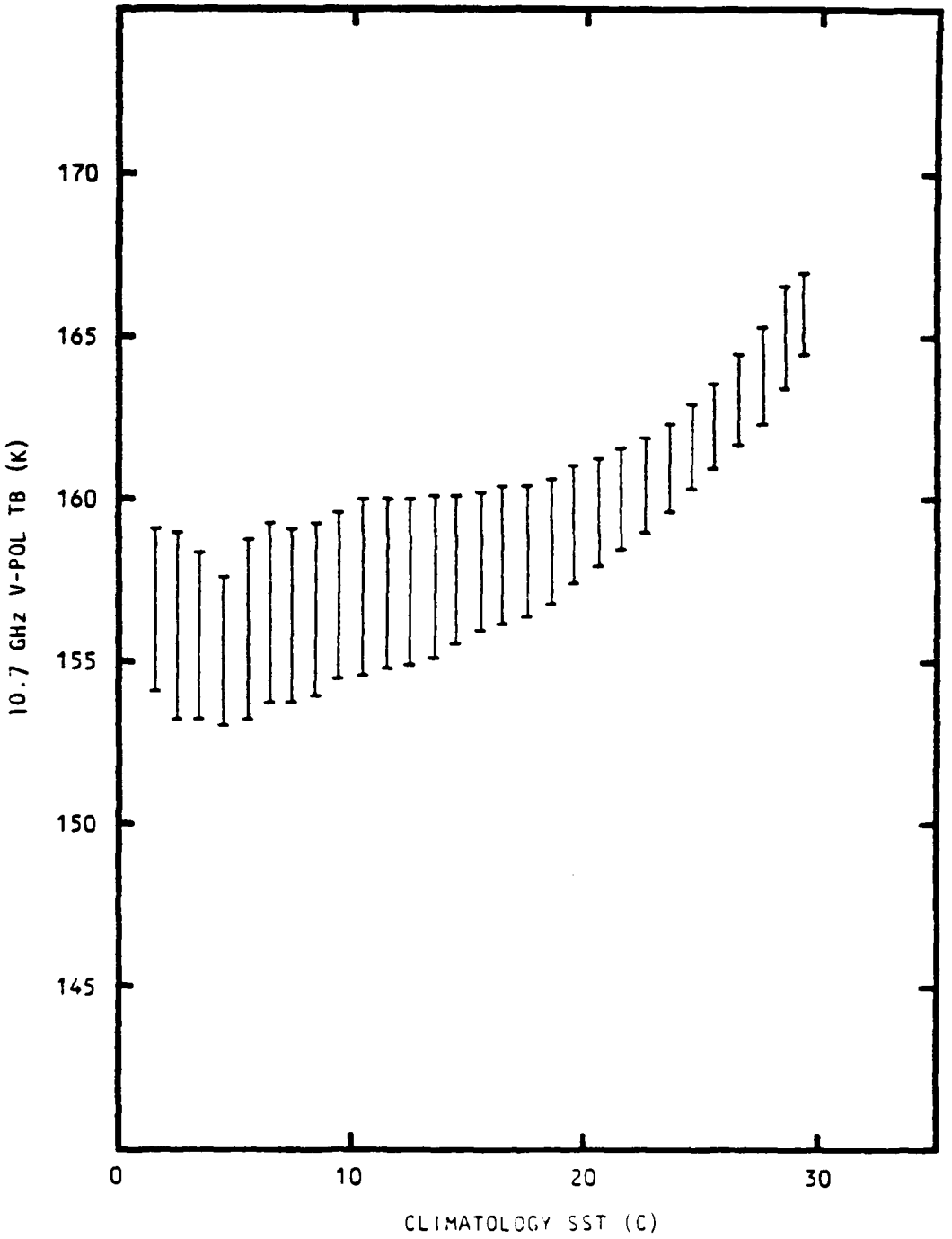

Fig. 5. Comparison of 10.7 GHz v-pol TB versus Climatology SST.

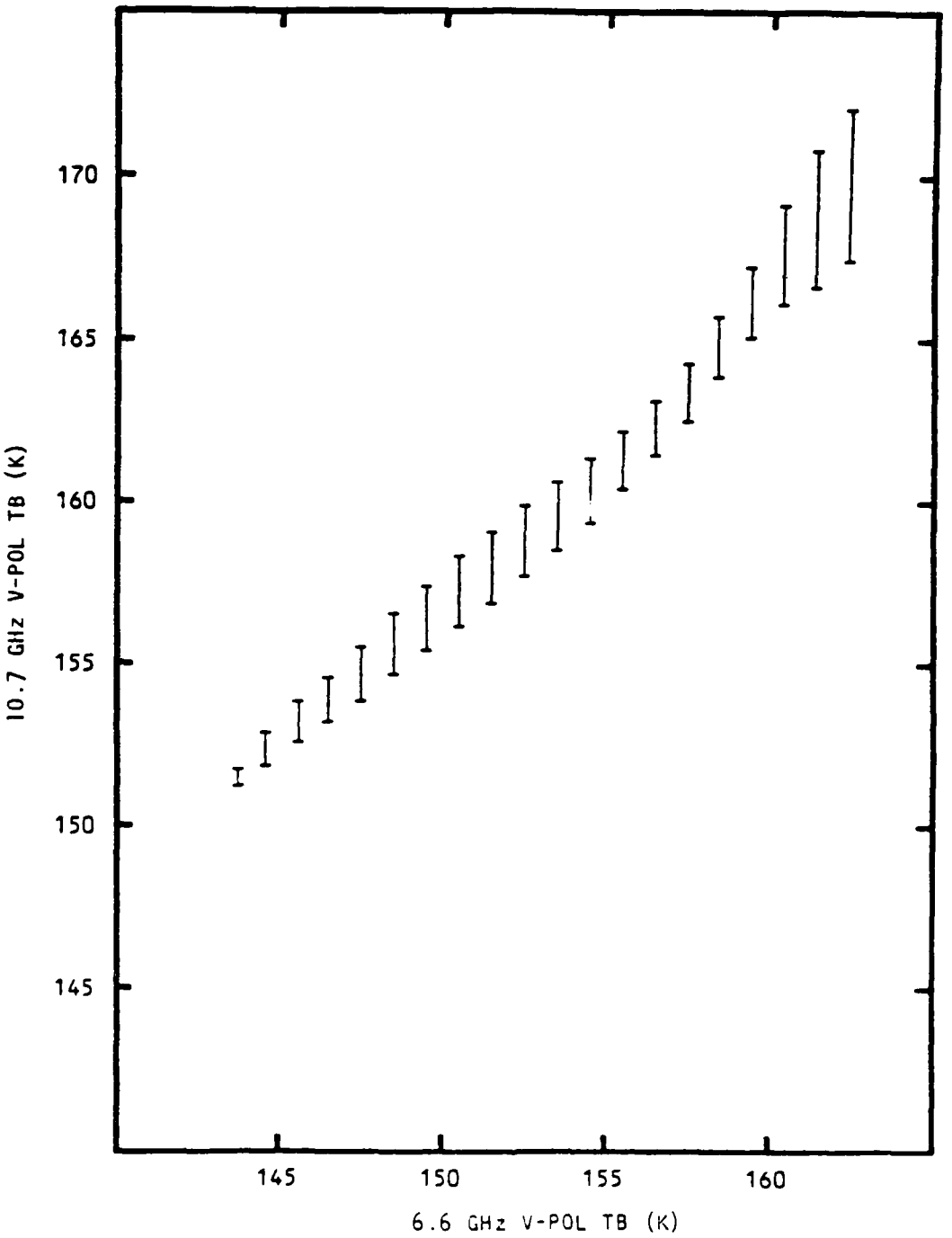

Fig. 6. Comparison of 10.7 GHz v-pol TB versus 6.6 GHz v-pol TB.

END

FILMED

8-84

DTIC